Continuum Mech. Thermodyn. (2013) 25:573–603
DOI 10.1007/s00161-012-0252-y

ORIGINAL ARTICLE

James G. McDonald · Clinton P. T. Groth

Towards realizable hyperbolic moment closures for viscous heat-conducting gas flows based on a maximum-entropy distribution

Received: 14 October 2011 / Accepted: 8 May 2012 / Published online: 9 June 2012

Abstract The ability to predict continuum and transition-regime flows by hyperbolic moment methods offers the promise of several advantages over traditional techniques. These methods offer an extended range of physical validity as compared with the Navier–Stokes equations and can be used for the prediction of many non-equilibrium flows with a lower expense than particle-based methods. Also, the hyperbolic first-order nature of the resulting partial differential equations leads to mathematical and numerical advantages. Moment equations generated through an entropy-maximization principle are particularly attractive due to their apparent robustness; however, their application to practical situations involving viscous, heat-conducting gases has been hampered by several issues. Firstly, the lack of closed-form expressions for closing fluxes leads to numerical expense as many integrals of distribution functions must be computed numerically during the course of a flow computation. Secondly, it has been shown that there exist physically realizable moment states for which the entropy-maximizing problem on which the method is based cannot be solved. Following a review of the theory surrounding maximum-entropy moment closures, this paper shows that both of these problems can be addressed in practice, at least for a simplified one-dimensional gas, and that the resulting flow predictions can be surprisingly good. The numerical results described provide significant motivations for the extension of these ideas to the fully three-dimensional case.

Keywords Gaskinetic theory · Hyperbolic moment closures · Transition-regime gasdynamics · Non-equilibrium flow

1 Introduction

Hyperbolic moment closures from gaskinetic theory offer the promise of robust and accurate methods for the prediction of viscous heat-conducting gas flows both in and out of local thermodynamic equilibrium. Such closures offer several advantages over traditional methods. An expanded solution vector allows a natural treatment of non-equilibrium effects and thus extends the regime of validity of the resulting moment equations past continuum-regime flows. This is important as traditional fluid equations are only valid in or very near the continuum

Communicated by Andreas Öchsner.

J. G. McDonald · C. P. T. Groth
University of Toronto Institute for Aerospace Studies, 4925 Dufferin Street, Toronto, ON M3H 5T6, Canada
E-mail: groth@utias.utoronto.ca

Present address:
J. G. McDonald (✉)
Rheinisch-Westfälische Technische Hochschule Aachen, Schinkelstr. 2, 52062 Aachen, Germany
E-mail: mcdonald@mathcces.rwth-aachen.de

regime. Non-equilibrium behaviour is a characteristic of gas flows in which the scales of interest are of a similar order as the mean free path of a gas particle. Such situations are typical of rarefied gas flows, micro-scale gas flows or hyper-sonic gas flows. Also, the hyperbolic nature of moment equations has several mathematical and computational advantages. Hyperbolic moment equations involve only first-order derivatives and are therefore very well suited to solution by the class of very successful Godunov-type finite-volume schemes that make use of adaptive mesh refinement (AMR) combined with treatments for embedded and moving boundaries and interfaces [15,19,35,38,46–48]. This is in contrast to other transport equations that have a partially elliptic nature and require the evaluation of second- or even higher-order derivatives. For hyperbolic systems, schemes of this type are robust, insensitive to irregularities in the computational grids, provide accurate resolution of discontinuities, and permit the systematic application of physically realistic boundary conditions. When coupled with AMR, they permit treatment of complex and evolving flow geometries and the resolution of highly disparate length scales while optimizing the usage of computational resources. They also have narrow stencils, making them suitable for implementation on massively parallel computer architectures [19,35,36,38,46–48]. Also, the necessity to calculate only first derivatives means that, for a given stencil or reconstruction, numerical schemes for the solution of moment equations can achieve one order higher spacial accuracy as compared to the solution of traditional fluid-dynamic equations such as the Navier–Stokes equations.

Unfortunately, all of the current standard moment closures can be said to be limited for one reason or another. For example, the original closure hierarchies due to Grad [10,17,18] result in moment equations that are hyperbolic for near-equilibrium flows. However, these PDEs can suffer from closure breakdown and loss of hyperbolicity, even for relatively small departures from equilibrium conditions and for physically realizable sets of macroscopic moments [7,56,57]. More recently, Struchtrup and Torrilhon have proposed regularized variants of the Grad moment-closure hierarchy based on a Chapman–Enskog expansion technique applied directly to the moment equations [51–53,58]. These regularized closures have proven most successful in providing insight into how different macroscopic moments interact for the formation of Knudsen-layer phenomena and their regularized behaviour results in smooth transitions for shocks (a desirable feature for high-speed applications, such as re-entry flows). However, the resulting transport equations for the moments are of mixed type (i.e., the moment fluxes are functions of the velocity moments and their derivatives) and formal hyperbolicity of the closures and all associated advantages are lost. Members of this regularized hierarchy maintain the issues related to hyperbolicity in the Grad closure on which they are based and closure breakdown can still be expected for larger deviations from local equilibrium. Diffusive closures constructed by applying the regularization technique of Struchtrup and Torrilhon [52] to a more robustly hyperbolic base closure could be constructed. This has already been investigated for expansion around the 10-moment Gaussian moment closure with good results [37]. If they were available, robust and affordable higher-order hyperbolic moment closures would allow similar models to be developed for more moments.

Alternative moment-closure techniques have been proposed based on the assumption that the approximate form for the distribution function corresponds to that of the maximum-entropy distribution [32,41]. The maximum-entropy distribution is defined to be the distribution that maximizes the physical entropy subject to the constraint that it be consistent with a given finite set of velocity moments. Moment closures obtained in this manner have many desirable mathematical properties including hyperbolicity, realizability of moments, and a definable entropy relation [32,41]. The lowest-order members of this hierarchy are the Maxwellian and Gaussian closures, both of which yield strictly hyperbolic moment equations and physically realizable moments. The Maxwellian closure leads to the well-known Euler equations governing inviscid adiabatic gas flow, while the Gaussian closure leads to a set of ten hyperbolic PDEs governing viscous adiabatic gas flow. Numerical solutions of the Gaussian closure using Godunov-type finite-volume schemes have been considered by Brown et al. [8,9], Le Tallec and Perlat [55], Suzuki and van Leer [54] and McDonald and Groth [19,35]. Numerical solution of these closures in a Discontinuous-Galerkin context has also been explored by Barth [4]. These early studies clearly illustrate some of the computational and modelling advantages of having a strictly hyperbolic and physically realizable treatment. Unfortunately, the simplicity and robustness of the two lowest-order members of this maximum-entropy hierarchy does not extend to higher-order closures. In fact, Junk has shown that any closure in this hierarchy that has moments of sufficiently high order to allow a treatment for heat transfer suffers from a region of non-realizability in moment space [29,30]. This result is particularly devastating as local equilibrium solutions can be shown to always lie on the boundary in moment space separating the valid region for the closure from the invalid region [30].

Recently, Schneider [22,49] has proposed an approach to dealing with the realizability of maximum-entropy closures. In this approach, regions of non-realizability are handled by relaxing the equality constraint

on some of the moment values. A maximum-entropy distribution function can then be found for a subset of the moments of interest. When Schneider's technique is followed, global hyperbolicity and realizability are recovered. Hauck et al. [22] have subsequently carried out a thorough mathematical analysis of this alternate approach to modifying maximum-entropy closures.

Alternately, hyperbolic moment closures that are not based on a maximum-entropy concept have been recently proposed by Torrilhon [57]. These closures are based on a Pearson-IV distribution function. Work in this area remains preliminary; it remains to be seen whether the resulting closures are truly globally hyperbolic and the quality of flow solutions produced by the resulting moment equations requires further study.

1.1 Scope of current study

This paper begins with a review of the derivation and relevant mathematical properties of maximum-entropy moment closures. Issues related to the use of higher-order maximum-entropy closures are also presented. It is then shown that the realizability issue associated with higher-order maximum-entropy closures can be removed through the use of a windowing technique. Hyperbolicity of the resulting moment equations can be maintained over a large region of moment space. Resulting flow simulations show that the predictions obtained from this technique can be remarkably good, especially for the prediction of shock-wave profiles. Shock profiles predicted using the resulting moment equations are shown to be far better than what should be expected by moment closures constructed in a way to ensure hyperbolicity but are not based on a physical principle such as entropy maximization. This work concludes with a presentation of a fitting technique for the one-dimensional, 5-moment, maximum-entropy system that leads to affordable moment equations with no noticeable loss of accuracy.

2 Gaskinetic theory and moment closures

Moment-closure techniques follow from the field of gaskinetic theory. In this theory, the microscopic particle nature of a gas is considered. A monatomic gas is represented by probability-density functions, $\mathcal{F}(x_i, v_i, t)$ that describe the number of particles at a given location, x_i, and time, t, having a particular gas velocity, v_i. Macroscopic properties of the gas are obtained by taking velocity moments of the distribution functions,

$$M(x_i,t) = \langle mV(v_i)\mathcal{F}(x_i,v_i,t)\rangle = \int_{-\infty}^{\infty}\int_{-\infty}^{\infty}\int_{-\infty}^{\infty} mV(v_i)\mathcal{F}(x_i,v_i,t)\mathrm{d}^3v, \tag{1}$$

where $M(x_i, t)$ is the macroscopic moment corresponding to the velocity weight $V(v_i)$ and m is the gas-particle mass. Typically, velocity weights are chosen to be monomials. Some commonly used lower-order moments include:

$$\begin{aligned} \rho &= \langle m\mathcal{F}\rangle, \\ u_i = \frac{\langle mv_i\mathcal{F}\rangle}{\rho}, &\qquad c_i = v_i - u_i, \\ \rho u_i u_j + P_{ij} = \langle mv_iv_j\mathcal{F}\rangle, &\qquad P_{ij} = \langle mc_ic_j\mathcal{F}\rangle, \\ \rho u_i u_j u_k + u_iP_{jk} + u_jP_{ik} + u_kP_{ij} + Q_{ijk} = \langle mv_iv_jv_k\mathcal{F}\rangle, &\qquad Q_{ijk} = \langle mc_ic_jc_k\mathcal{F}\rangle, \end{aligned}$$

where ρ is the mass density, u_i is the bulk velocity, c_i is the random component of the gas-particle velocity, P_{ij} is an anisotropic pressure tensor, and Q_{ijk} is the generalized heat-flux tensor. The pressure and heat-flux tensors are related to the more familiar thermodynamic pressure and heat-flux vector through the contractions $p = \frac{1}{3}P_{ii}$ and $q_i = \frac{1}{2}Q_{ijj}$. Also, the deviatoric fluid-stress tensor is related to the pressure tensor as $\tau_{ij} = \delta_{ij}p - P_{ij}$. Following this method, moments of arbitrarily high order can be taken; however, as the order of a moment becomes higher, its physical significance can becomes less and less intuitively obvious.

The evolution of the distribution function, $\mathcal{F}$, is described by the well-known Boltzmann equation [10,11, 17,41,51],

$$\frac{\partial\mathcal{F}}{\partial t} + v_i\frac{\partial\mathcal{F}}{\partial x_i} = \frac{\delta\mathcal{F}}{\delta t}, \tag{2}$$

shown here in the absence of external acceleration fields. The term on the right-hand side of Eq. (2) is the collision integral and represents the time rate of change of the distribution function produced by inter-particle collisions. By taking moments of this distribution function, equations describing the evolution of macroscopic moments can be obtained. The result is known as Maxwell's equation of change,

$$\frac{\partial}{\partial t}\left\langle mV(v_i)\mathcal{F}\right\rangle + \frac{\partial}{\partial x_i}\left\langle v_i V(v_i)\mathcal{F}\right\rangle = \left\langle mV(v_i)\frac{\delta\mathcal{F}}{\delta t}\right\rangle. \tag{3}$$

Typically, the evolution of several macroscopic moments is deemed important for a situation. A vector containing these moments, $\boldsymbol{U}$, is therefore defined with a corresponding vector of velocity weights, $\boldsymbol{V}$, such that

$$\boldsymbol{U} = \langle m\boldsymbol{V}\mathcal{F}\rangle. \tag{4}$$

Substituting the vector $\boldsymbol{V}$ into Eq. (3) results in a system of moment equations,

$$\frac{\partial}{\partial t}\left\langle m\boldsymbol{V}\mathcal{F}\right\rangle + \frac{\partial}{\partial x_i}\left\langle mv_i\boldsymbol{V}\mathcal{F}\right\rangle = \frac{\partial \boldsymbol{U}}{\partial t} + \frac{\partial \boldsymbol{F}_i}{\partial x_i} = \left\langle m\boldsymbol{V}\frac{\delta\mathcal{F}}{\delta t}\right\rangle, \tag{5}$$

where $\boldsymbol{F}_i$ is the flux dyad corresponding to the conserved moments contained in $\boldsymbol{U}$. Unfortunately, this system is not closed. The time rate of change of each moment in $\boldsymbol{U}$ is dependent on the spacial divergence of a moment of one order higher in velocity, that moment's flux. In general, the flux of the highest-order moments in $\boldsymbol{U}$ is therefore not known. The term on the right-hand side, the effect of inter-particle collisions on the moments of interest, is also not known in general. As it is the modelling of the left-hand side that is of primary interest in the present work, a simplified relaxation-time model will later be adopted for the collision operator that results in closed-form expressions.

2.1 Moment closure

The technique of moment closure involves adopting an assumed form for the distribution function, $\mathcal{F}$, in terms of a limited number of free parameters, or closure coefficients, $\boldsymbol{\alpha}$. These coefficients are then set such that Eq. (4) is satisfied. The number of free parameters must therefore be equal to the number of entries in $\boldsymbol{U}$. In this way, all higher-order moments become a function of the known lower-order moments, and the system of moment equations is closed. In general, it is not known exactly which moments are required to properly describe a particular non-equilibrium process. Work has been done to study the order of magnitude of terms in moment equations in terms of the Knudsen number by Müller et al. through their "consistent order extended thermodynamics" [40] and later by Struchtrup with his "order of magnitude method" [50]. Clearly, employing more moments provides additional freedom to more accurately represent higher-Knudsen-number non-equilibrium behaviour.

The most well-known assumed form for the distribution function is the Grad-type polynomial series expansions [18] having the form

$$\mathcal{F} = \mathcal{M}\left[\boldsymbol{\alpha}^{\mathrm{T}}\mathbf{V}\right], \tag{6}$$

where the expansion is performed about the equilibrium solution or Maxwellian distribution function, $\mathcal{M}$, given by

$$\mathcal{M} = \frac{\rho}{m\left(2\pi p/\rho\right)^{3/2}} e^{\left(-\frac{1}{2}\frac{\rho c_i c_i}{p}\right)}, \tag{7}$$

Originally, Grad considered both 13- and 20-moment closures. Subsequently, extensions to many moments have been considered by others [41,51]. It should be noted Grad expressed the polynomial in Eq. (6), $\boldsymbol{\alpha}^{\mathrm{T}}\mathbf{V}$, as a sum of Hermite polynomials. This decouples the dependence of the closure coefficients and greatly simplifies the derivation. This technique is common practice.

It is an unfortunate fact that members of the Grad hierarchy suffer from several problems. Firstly, the distribution function defined in Eq. (6) is not always positive. It is therefore not a properly defined probability-density function. Secondly, for modest departures from local equilibrium, it is possible for the resulting moment equations to become non-hyperbolic [7,56,57]. As a consequence, the moment equations may no longer be well posed for initial-value problems.

3 Maximum-entropy moment closures

An alternative approach to obtaining closure of the moment equations is to assume the distribution function is such that it has the maximum physical entropy while remaining consistent with the macroscopic moments in $\boldsymbol{U}$ [12,32,41,51]. For classical gases, for which the entropy density is know to be $\langle \mathcal{F} \ln \mathcal{F} \rangle$, this assumption leads to distribution functions of the form

$$\mathcal{F} = e^{\boldsymbol{\alpha}^{\mathrm{T}} \mathbf{V}} \tag{8}$$

This distribution function is positive valued, and, through careful selection of the generating velocity weights in $\boldsymbol{V}$, it can be assured that the distribution remains finite [32]. Moreover, the hyperbolicity of the resulting moment equations can be demonstrated [12,32,41,51]. This can be done by defining density and flux potentials as

$$h(\boldsymbol{\alpha}) = \left\langle m e^{\boldsymbol{\alpha}^{\mathrm{T}} \mathbf{V}} \right\rangle, \quad f_i(\boldsymbol{\alpha}) = \left\langle m v_i e^{\boldsymbol{\alpha}^{\mathrm{T}} \mathbf{V}} \right\rangle. \tag{9}$$

The conserved moments and fluxes can then be expressed as

$$h_{,\boldsymbol{\alpha}} = \frac{\partial h}{\partial \boldsymbol{\alpha}} = \left\langle m \mathbf{V} e^{\boldsymbol{\alpha}^{\mathrm{T}} \mathbf{V}} \right\rangle, \quad f_{i,\boldsymbol{\alpha}} = \frac{\partial f_i}{\partial \boldsymbol{\alpha}} = \left\langle m v_i \mathbf{V} e^{\boldsymbol{\alpha}^{\mathrm{T}} \mathbf{V}} \right\rangle, \tag{10}$$

and the moment equations of Eq. (5) can then be written as

$$\frac{\partial}{\partial t} \left(h_{,\boldsymbol{\alpha}} \right) + \frac{\partial}{\partial x_i} f_{i,\boldsymbol{\alpha}} = \mathbf{S}(\boldsymbol{\alpha}), \tag{11}$$

where $\mathbf{S}(\boldsymbol{\alpha}) = \langle \boldsymbol{V} \delta \mathcal{F} / \delta t \rangle$ is the source term associated with collisional processes. The terms $h_{,\boldsymbol{\alpha}}$ and $f_{i,\boldsymbol{\alpha}}$ can be differentiated again to give

$$h_{,\boldsymbol{\alpha}\boldsymbol{\alpha}} = \left\langle m \mathbf{V}\mathbf{V}^{\mathrm{T}} e^{\boldsymbol{\alpha}^{\mathrm{T}} \mathbf{V}} \right\rangle, \tag{12}$$

and

$$f_{i,\boldsymbol{\alpha}\boldsymbol{\alpha}} = \left\langle m v_i \, \mathbf{V}\mathbf{V}^{\mathrm{T}} e^{\boldsymbol{\alpha}^{\mathrm{T}} \mathbf{V}} \right\rangle. \tag{13}$$

The moment equations above can then be re-expressed as

$$h_{,\boldsymbol{\alpha}\boldsymbol{\alpha}} \frac{\partial \boldsymbol{\alpha}}{\partial t} + f_{i,\boldsymbol{\alpha}\boldsymbol{\alpha}} \frac{\partial \boldsymbol{\alpha}}{\partial x_i} = \mathbf{S}(\boldsymbol{\alpha}). \tag{14}$$

Equation (14) describes the time evolution of the closure coefficients for a maximum-entropy distribution. Hyperbolicity of this system is assured by the symmetry of $f_{i,\boldsymbol{\alpha}\boldsymbol{\alpha}}$ and symmetric positive definiteness of $h_{,\boldsymbol{\alpha}\boldsymbol{\alpha}}$ [14,16,32]. The positive definiteness of $h_{,\boldsymbol{\alpha}\boldsymbol{\alpha}}$ is known because for any vector $\mathbf{w}$,

$$\mathbf{w}^{\mathrm{T}} h_{,\boldsymbol{\alpha}\boldsymbol{\alpha}} \mathbf{w} = \left\langle \mathbf{w}^{\mathrm{T}} \mathbf{V}\mathbf{V}^{\mathrm{T}} \mathbf{w} e^{\boldsymbol{\alpha}^{\mathrm{T}} \mathbf{V}} \right\rangle = \left\langle \left(\mathbf{w}^{\mathrm{T}} \mathbf{V} \right)^2 e^{\boldsymbol{\alpha}^{\mathrm{T}} \mathbf{V}} \right\rangle \geq 0. \tag{15}$$

and hence $h_{,\boldsymbol{\alpha}\boldsymbol{\alpha}}$ is both symmetric and positive definite.

3.1 Members of the maximum-entropy hierarchy

The lowest-order member of the maximum-entropy hierarchy is generated using the velocity-weight vector $\boldsymbol{V} = [1, v_i, v_i v_i]^{\mathrm{T}}$. This leads to the well-known Euler equations for compressible gas flow, a 5-moment model. The next-lowest-order member of the hierarchy is generated using the vector $\boldsymbol{V} = [1, v_i, v_i v_j]^{\mathrm{T}}$. This choice leads to a system of ten moment equations known as the Gaussian moment closure. It provides a treatment for fluid stresses through the definition of an anisotropic pressure tensor. The Gaussian distribution appears to have been first derived in early work by Maxwell [34] and then re-discovered in subsequent but independent research by both Schlüter [42,23] and Holway [24–27]. Numerical computations have demonstrated that this model can be very successful for continuum and transition-regime flows for which heat transfer is not important [4,8,9,19,35,54,55]. The closure's inability to predict heat-transfer phenomena is due to the fact that the Gaussian closure always predicts zero heat flux by construction.

Higher-order members of the maximum-entropy hierarchy do provide a treatment for heat transfer; however, there is a problem. When the polynomial in the exponential of Eq. (8) contains super-quadratic terms, closed-form expressions for the integrals of the distribution function are not possible. This means expressions for the closure coefficients such that Eq. (4) is satisfied cannot be found. The closing fluxes can therefore not be expressed as a closed-form expression of the conserved moments.

It is, however, possible to relate the moments and closure coefficients through an iterative procedure [32,55]. This is done by first defining a function

$$J(\boldsymbol{\alpha}) = \left\langle e^{\boldsymbol{\alpha}^{\mathrm{T}}\mathbf{V}} \right\rangle - \boldsymbol{\alpha}^{\mathrm{T}}\boldsymbol{U}. \tag{16}$$

This function has an extremum when

$$\frac{\partial}{\partial \boldsymbol{\alpha}} J(\boldsymbol{\alpha}) = \left\langle \mathbf{V} e^{\boldsymbol{\alpha}^{\mathrm{T}}\mathbf{V}} \right\rangle - \boldsymbol{U} = 0. \tag{17}$$

This is exactly the condition of consistency from Eq. (4). Moreover, the Hessian of $J(\boldsymbol{\alpha})$ is equal to the Hessian of the density potential, $h(\boldsymbol{\alpha})$, as shown in Eq. (12); this has already been shown to be positive definite. The function, $J(\boldsymbol{\alpha})$, therefore, has at most one extremum that is obtained when $\boldsymbol{\alpha}$ and $\boldsymbol{U}$ are consistent. This convex optimization problem can be solved using a Newton-like technique; however, in the course of this synchronization, the moments of the distribution function must be calculated numerically for the construction of the gradient and Hessian of $J(\boldsymbol{\alpha})$. The computational domain for these integrations stretches to infinity in all directions of velocity space, adding obvious numerical difficulties and expense.

There is a somewhat more subtle issue that arises in the use of higher-order, maximum-entropy moment closures. Junk has shown that for all generating vectors, $\boldsymbol{V}$, containing super-quadratic velocity weights, there exist physically realizable moment states for which the entropy-maximization problem does not have a solution [29,30]. In these regions, the entire framework of maximum-entropy moment closure breaks down. Seemingly more devastating, the equilibrium distribution function always lies on the boundary separating the realizable and non-realizable regions.

Although lower-order members of the maximum-entropy moment-closure hierarchy have proven very successful [19,35,36,38], the inability to express moment fluxes in closed form and the presence of regions of non-realizability has seriously hampered efforts to make practical use of higher-order maximum-entropy moment closures. In what follows, a simplified one-dimensional moment system is used to investigate the practical implications of these issues. It is shown that both issues can be handled, at least for this simplified model and that flow predictions are surprisingly good.

4 Mathematical structure of one-dimensional moment closures

In order to examine the modelling issues associated with higher-order maximum-entropy closures, kinetic theory applied to a one-dimensional gas is considered. A one-dimensional gas is defined as a gas whose molecules can only have velocities in one space dimension. In the case of no external acceleration fields, the Boltzmann equation for a one-dimensional gas simplifies to

$$\frac{\partial \mathcal{F}}{\partial t} + v\frac{\partial \mathcal{F}}{\partial x} = \frac{\delta \mathcal{F}}{\delta t}. \tag{18}$$

The independent variables, velocity, v, and position, x, are now scalars. Similarly, Maxwell's equation of change simplifies to

$$\frac{\partial}{\partial t}\langle m\boldsymbol{V}\mathcal{F}\rangle + \frac{\partial}{\partial x}\langle mv\boldsymbol{V}\mathcal{F}\rangle = \left\langle \boldsymbol{V}\frac{\delta\mathcal{F}}{\delta t}\right\rangle. \tag{19}$$

An N-moment system of moment equations corresponding to velocity weights $\boldsymbol{V}$ can be written as

$$\frac{\partial \mathbf{U}}{\partial t} + \frac{\partial \mathbf{F}}{\partial x} = \mathbf{S}, \tag{20}$$

where $\mathbf{F}$ is now a vector rather than a dyad and $\mathbf{S}$ is the local source vector arising from inter-particle collisions.

One-dimensional moment equations have some remarkable mathematical properties that can be examined by rewriting Eq. (20) as

$$\frac{\partial \mathbf{U}}{\partial t} + \frac{\partial \mathbf{F}}{\partial \mathbf{U}}\frac{\partial \mathbf{U}}{\partial x} = \mathbf{S}. \tag{21}$$

When polynomial velocity weights are used to generate the moment equations, the flux of one moment will be a moment that is of one order higher. For this simplified one-dimensional situation, the fact that velocity is a scalar means that there is only one moment of each order and the flux Jacobian, $\frac{\partial \mathbf{F}}{\partial \mathbf{U}}$, has the structure of a companion matrix having the form

$$\frac{\partial \mathbf{F}}{\partial \mathbf{U}} = \begin{bmatrix} 0 & 1 & 0 & 0 & \cdots & 0 \\ 0 & 0 & 1 & 0 & \cdots & 0 \\ 0 & 0 & 0 & 1 & \cdots & 0 \\ \vdots & \vdots & \vdots & \ddots & \ddots & \vdots \\ 0 & 0 & 0 & 0 & \cdots & 1 \\ a_0 & a_1 & a_2 & a_3 & \cdots & a_{(N-1)} \end{bmatrix}. \tag{22}$$

Companion matrices are interesting as their characteristic equation, $p(\lambda)$, has the form

$$p(\lambda) = a_0 + a_1\lambda + a_2\lambda^2 + a_3\lambda^3 + \cdots + a_{(N-1)}\lambda^{(N-1)} - \lambda^N. \tag{23}$$

The N roots of this equation, λ_n, represent the N eigenvalues of the matrix. Moreover, the matrix with right eigenvectors as columns that corresponds to a companion matrix is a Vandermonde matrix of the form

$$\bar{\mathbf{R}} = \begin{bmatrix} 1 & 1 & 1 & \cdots & 1 \\ \lambda_0 & \lambda_1 & \lambda_2 & \cdots & \lambda_{(N-1)} \\ \lambda_0^2 & \lambda_1^2 & \lambda_2^2 & \cdots & \lambda_{(N-1)}^2 \\ \lambda_0^3 & \lambda_1^3 & \lambda_2^3 & \cdots & \lambda_{(N-1)}^3 \\ \vdots & \vdots & \vdots & \ddots & \vdots \\ \lambda_0^{(N-1)} & \lambda_1^{(N-1)} & \lambda_2^{(N-1)} & \cdots & \lambda_{(N-1)}^{(N-1)} \end{bmatrix} \tag{24}$$

It is known that for all hyperbolic systems, there exists a diagonal matrix, $\mathbf{W}$, containing eigenvector scalings, w_i, such that systems of the form shown in Eq. (21) can be written in symmetric form as

$$\bar{\mathbf{H}}\frac{\partial \boldsymbol{\alpha}}{\partial t} + \bar{\mathbf{J}}\frac{\partial \boldsymbol{\alpha}}{\partial x} = \mathbf{S}, \tag{25}$$

where $\bar{\mathbf{H}} = \bar{\mathbf{R}}\bar{\mathbf{W}}\bar{\mathbf{R}}^{\mathrm{T}}$ and $\bar{\mathbf{J}} = \bar{\mathbf{R}}\bar{\mathbf{W}}\bar{\boldsymbol{\Lambda}}\bar{\mathbf{R}}^{\mathrm{T}}$ are symmetric matrices while $\boldsymbol{\alpha}$ are the so-called entropy variables and $\boldsymbol{\Lambda}$ is a diagonal matrix containing the eigenvalues of the flux Jacobian [3]. Equation (14) shows that, for maximum-entropy moment closures, the symmetrizing variables are in fact the closure coefficients. These coefficients are also the entropy variables for the system, while $\bar{\mathbf{H}}$ and $\bar{\mathbf{J}}$ are the Hessians of the density and flux potentials, as given earlier in Eqs. 12 and 13.

For the one-dimensional case, both of the Hessians $\bar{\mathbf{H}}$ and $\bar{\mathbf{J}}$ are Hankel matrices whose entries are moments of the maximum-entropy distribution function. That is, they have the form

$$\bar{\mathbf{H}} = \begin{bmatrix} U_0 & U_1 & U_2 & \cdots & U_{N-1} \\ U_1 & U_2 & U_3 & \cdots & U_N \\ U_2 & U_3 & U_4 & \cdots & \vdots \\ \vdots & \vdots & \vdots & \ddots & U_{2N-3} \\ U_{N-1} & U_N & \cdots & U_{2N-3} & U_{2N-2} \end{bmatrix}, \tag{26}$$

and

$$\bar{\mathbf{J}} = \begin{bmatrix} U_1 & U_2 & U_3 & \cdots & U_N \\ U_2 & U_3 & U_4 & \cdots & U_{N+1} \\ U_3 & U_4 & U_5 & \cdots & \vdots \\ \vdots & \vdots & \vdots & \ddots & U_{2N-2} \\ U_N & U_{N+1} & \cdots & U_{2N-2} & U_{2N-1} \end{bmatrix}, \tag{27}$$

where here U_n is the nth-order conserved moment.

It is at this point that a very interesting property of one-dimensional maximum-entropy moment closures can be demonstrated. By carrying out the matrix multiplication $\bar{\mathbf{H}} = \bar{\mathbf{R}}\bar{\mathbf{W}}\bar{\mathbf{R}}^{\mathrm{T}}$ and $\bar{\mathbf{J}} = \bar{\mathbf{R}}\bar{\mathbf{W}}\bar{\mathbf{\Lambda}}\bar{\mathbf{R}}^{\mathrm{T}}$ with $\bar{\mathbf{R}}$, $\bar{\mathbf{H}}$ and $\bar{\mathbf{J}}$ defined by Eqs. (24), (26) and (27), respectively, it can be seen that the conserved velocity moments can be expressed as

$$U_n = \sum_{i=0}^{(N-1)} w_i \lambda_i^n \quad \text{for} \quad n \leq 2N-1. \tag{28}$$

That is, the eigenvalues of the system are the N Gauss quadrature points for which the zeroth to the $(2N-1)$th moments of the maximum-entropy velocity distribution function are captured exactly and the N eigenvector scaling factors, w_i, are in fact the corresponding weights for the numerical integration rule. The relationship between the Vandermonde decomposition of a Hankel matrix and Gauss quadrature rules has been known for some time [6,13]. However, this surprising relationship between Gauss quadrature points and the eigenvalues of a one-dimensional maximum-entropy moment system does not seem to have been discussed elsewhere in the published literature pertaining to moment closures for kinetic theory.

5 Navier–Stokes-like equations for a one-dimensional gas

In order to assess the advantages that the proposed hyperbolic moment closures have over traditional fluid-dynamic equations, a one-dimensional equivalent to the Navier–Stokes equations will be examined. The derivation of these equations for the one-dimensional gas is detailed here.

5.1 One-dimensional Maxwell–Boltzmann distribution and 3-moment equilibrium closure

The corresponding equilibrium Maxwell–Boltzmann distribution function for a one-dimensional gas can be written as

$$\mathcal{M} = \frac{\rho}{m}\sqrt{\frac{\rho}{2\pi p}}\exp\left(-\frac{\rho}{2p}c^2\right). \tag{29}$$

This distribution function has moments:

$$\begin{aligned} &\rho = \langle m\mathcal{M}\rangle, && \\ &\rho u = \langle mv\mathcal{M}\rangle, && 0 = \langle mc\mathcal{M}\rangle, \\ &\rho u^2 + p = \langle mv^2\mathcal{M}\rangle, && p = \langle mc^2\mathcal{M}\rangle, \\ &\rho u^3 + 3up = \langle mv^3\mathcal{M}\rangle, && 0 = \langle mc^3\mathcal{M}\rangle, \\ &\rho u^4 + 6u^2p + \frac{3p^2}{\rho} = \langle mv^4\mathcal{M}\rangle, && \tfrac{3p^2}{\rho} = \langle mc^4\mathcal{M}\rangle, \\ &\rho u^5 + 10u^3p + 15u\tfrac{p^2}{\rho} = \langle mv^5\mathcal{M}\rangle, && 0 = \langle mc^5\mathcal{M}\rangle. \end{aligned} \tag{30}$$

If this equilibrium distribution function is substituted into Maxwell's equation of change, the result is a three moment system that can be written as

$$\frac{\partial \rho}{\partial t} + \frac{\partial}{\partial x}(\rho u) = 0, \tag{31}$$

$$\frac{\partial}{\partial t}(\rho u) + \frac{\partial}{\partial x}\left(\rho u^2 + p\right) = 0, \tag{32}$$

$$\frac{\partial}{\partial t}\left(\rho u^2 + p\right) + \frac{\partial}{\partial x}\left(\rho u^3 + 3up\right) = 0. \tag{33}$$

This 3-moment Euler system describes one-dimensional gas flow in thermodynamic equilibrium. The system has wave speeds $u + a$, u and $u - a$ with $a = \sqrt{3p/\rho}$.

5.2 Collision operators for a one-dimensional gas

Traditionally, when moment closures are used to reduce the dimensionality of the Boltzmann equation, two sources of error are incurred. Firstly, there is the obvious error caused by restricting the distribution function to having a prescribed form. In practice, however, it is also usually necessary to model the collision operator in some way. When accessing the quality of a particular moment closure, it is most prudent to separate these two errors and study only the error directly associated with the closure. Errors caused by the collision operator should be seen as a separate issue. To this end, the same collision operator will be used for all models in this work, including directly computed solutions to the Boltzmann equation. A very simple and common collision model is the BGK or relaxation collision operator [5]. This operator can be written as

$$\frac{\delta \mathcal{F}}{\delta t} = -\frac{\mathcal{F} - \mathcal{M}}{\tau}. \tag{34}$$

It predicts that a general non-equilibrium distribution function, $\mathcal{F}$, will relax towards the equilibrium distribution, $\mathcal{M}$, over a timescale τ.

5.3 Chapman–Enskog expansion for a one-dimensional gas and Navier–Stokes model

The Navier–Stokes-like equations for a one-dimensional gas can be derived through a Chapman–Enskog expansion of the moment equations. First, it is convenient to define the fourth moment

$$k = \left\langle mc^4 \mathcal{F} \right\rangle - \left\langle mc^4 \mathcal{M} \right\rangle = \left\langle mc^4 \mathcal{F} \right\rangle - \frac{3p}{\rho} = r - \frac{3p}{\rho}, \tag{35}$$

which is the deviation of the random-velocity fourth moment $r = \langle mc^4 \mathcal{F} \rangle$ from its value in thermodynamic equilibrium. Next, the third-order random-velocity heat-transfer moment $q = \langle mc^3 \mathcal{F} \rangle$ and k are written as perturbative expansions about their equilibrium value as

$$q = q^{(\mathcal{M})} + \epsilon q^{(1)} + \epsilon^2 q^{(2)} + \epsilon^3 q^{(3)} + \cdots, \tag{36}$$

$$k = k^{(\mathcal{M})} + \epsilon k^{(1)} + \epsilon^2 k^{(2)} + \epsilon^3 k^{(3)} + \cdots. \tag{37}$$

The moment equation for the second-order moment $\langle mv^2 \mathcal{F} \rangle$ can be written for a general distribution function as

$$\frac{\partial}{\partial t}\left(\rho u^2 + p\right) + \frac{\partial}{\partial x}\left(\rho u^3 + 3up + q\right) = 0. \tag{38}$$

It is the moment q that corresponds to the heat flux and is not present in the equilibrium Euler equations for a one-dimensional gas [Eqs. (31)–(33)]. The moment equation that describes the evolution of q can then be written with a scaled BGK collision term as

$$\frac{\partial q}{\partial t} + 4q\frac{\partial u}{\partial x} + u\frac{\partial q}{\partial x} + 3p\frac{\partial}{\partial x}\left(\frac{p}{\rho}\right) + \frac{\partial k}{\partial x} = -\frac{q}{\epsilon\tau}. \tag{39}$$

Here, the smallness parameter ϵ on the right-hand side of the equations signifies an assumption that any deviation from equilibrium is attenuated very rapidly by collisional processes. The expansions for q and k, Eqs. (36) and (37), are now inserted and terms of equal order in ϵ are gathered. Once this is done, it can be seen that the zeroth-order terms lead to the equations

$$q^{(\mathcal{M})} = 0, \tag{40}$$

and

$$k^{(\mathcal{M})} = 0, \tag{41}$$

as required. By collecting first-order terms, the approximation to the heat-flux moment is then found to be

$$q^{(1)} = -3p\tau \frac{\partial}{\partial x}\left(\frac{p}{\rho}\right). \tag{42}$$

This expression can then be combined with Eq. (38) to yield the one-dimensional Navier–Stokes-like equations that will be used as a representative continuum-regime model for comparison in this work. The resulting transport equations can be summarized as follows:

$$\frac{\partial \rho}{\partial t} + \frac{\partial}{\partial x}(\rho u) = 0, \tag{43}$$

$$\frac{\partial}{\partial t}(\rho u) + \frac{\partial}{\partial x}\left(\rho u^2 + p\right) = 0, \tag{44}$$

$$\frac{\partial}{\partial t}\left(\rho u^2 + p\right) + \frac{\partial}{\partial x}\left(\rho u^3 + 3up\right) - \frac{\partial}{\partial x}\left(3p\tau \frac{\partial}{\partial x}\left(\frac{p}{\rho}\right)\right) = 0. \tag{45}$$

6 A 5-moment one-dimensional maximum-entropy moment closure

The lowest-order member of the Levermore hierarchy for a one-dimensional gas that provides a treatment for heat transfer is a 5-moment system. The vector of generating weights is $\mathbf{V} = [1, v, v^2, v^3, v^4]^{\mathrm{T}}$; the resulting maximum-entropy distribution function is

$$\mathcal{F} = e^{(\alpha_0 + \alpha_1 v + \alpha_2 v^2 + \alpha_3 v^3 + \alpha_4 v^4)}, \tag{46}$$

and the corresponding moment equations are

$$\frac{\partial \rho}{\partial t} + \frac{\partial}{\partial x}(\rho u) = 0, \tag{47}$$

$$\frac{\partial}{\partial t}(\rho u) + \frac{\partial}{\partial x}\left(\rho u^2 + p\right) = 0, \tag{48}$$

$$\frac{\partial}{\partial t}\left(\rho u^2 + p\right) + \frac{\partial}{\partial x}\left(\rho u^3 + 3up + q\right) = 0, \tag{49}$$

$$\frac{\partial}{\partial t}\left(\rho u^3 + 3up + q\right) + \frac{\partial}{\partial x}\left(\rho u^4 + 6u^2 p + 4uq + r\right) = -\frac{q}{\tau}, \tag{50}$$

$$\begin{aligned}&\frac{\partial}{\partial t}\left(\rho u^4 + 6u^2 p + 4uq + r\right) + \frac{\partial}{\partial x}\left(\rho u^5 + 10u^3 p + 10u^2 q + 5ur + s\right)\\ &\quad = -\frac{1}{\tau}\left(4uq + r - 3\frac{p^2}{\rho}\right).\end{aligned} \tag{51}$$

It is the fifth-order random-velocity moment $s = \langle mc^5\mathcal{F}\rangle$ that is not a member of the solution vector and must therefore be determined from a closure relation. As explained earlier, the standard BGK relaxation operator is used to represent the collision terms.

The distribution function of Eq. (46) has been studied previously in the field of probability [1,33,43,44]. It is known that moments of this distribution function, $\langle mv^n\mathcal{F}\rangle$, cannot be expressed as a closed-form function of the closure coefficients. This means that the closing flux cannot be expressed as an explicit function of the lower-order moments that are present in the solution vector. It is for this reason that the entropy-maximization problem must be solved numerically at every time a flux is needed in any numerical-solution procedure for the moment equations.

Again, this is not the only hindrance to the use of such closures. As with all higher-order maximum-entropy closures, Junk has shown that there exist physically realizable moment states for this system for which the entropy-maximization problem has no solution. In these regions, the entire mathematical framework of the maximum-entropy moment closure breaks down [29,30].

7 Moment realizability

The term moment realizability refers to the existence of a function with certain specified properties that correspond to a given set of moments. Although a finite set of velocity moments cannot in general be used to uniquely specify a distribution function and multiple distributions that share the same N moments can usually be defined, in assessing moment realizability the question is asked whether any distribution function with specified properties can correspond to the given set of moments.

7.1 Physical realizability

The question of physical realizability is a question of whether a positive probability-density function exists that corresponds to certain prescribed moments. For any given set of velocity weights, $\mathbf{M} = m[1, v_i, v_iv_j, \ldots]^{\mathrm{T}}$, one can construct polynomials, $\mathcal{P}(v_i)$, as

$$\mathcal{P}(v_i) = \boldsymbol{a}^{\mathrm{T}}\mathbf{M}, \tag{52}$$

where $\boldsymbol{a}$ is a column vector containing the coefficients of the polynomial. For any positive-valued distribution, $\mathcal{F}$, and polynomial, $\mathcal{P}$, it is clearly a requirement that

$$\langle||\mathcal{P}(v_i)||^2\mathcal{F}\rangle \;=\; \boldsymbol{a}^{\mathrm{T}}\langle\mathbf{M}\mathbf{M}^{\mathrm{T}}\mathcal{F}\rangle\boldsymbol{a} \;=\; \boldsymbol{a}^{\mathrm{T}}\bar{\mathbf{Y}}\boldsymbol{a} \;\geq\; 0, \tag{53}$$

and thus the moments present in the real symmetric matrix $\bar{\mathbf{Y}}$, given by

$$\bar{\mathbf{Y}} = \langle\mathbf{M}\mathbf{M}^{\mathrm{T}}\mathcal{F}\rangle, \tag{54}$$

are physically realizable when this matrix is positive definite. It should be noted that in assessing the physical realizability of a given moment state, the vector of velocity weights, $\mathbf{M}$, does not only need to be equal to the vector of generating weights, $\mathbf{V}$, of the known moments. In fact, for a distribution function to be realizable, the matrix $\bar{\mathbf{Y}}$ must be positive definite for every possible choice of $\mathbf{M}$. In order to assess the physical realizability of a specific moment state, the vector, $\mathbf{M}$, which will lead to the known moments being included in $\bar{\mathbf{Y}}$, should be chosen.

For situations in which $\bar{\mathbf{Y}}$ is not positive definite, it follows that the velocity moments it contains are not consistent with any possible positive-valued distribution function and, hence, are not physically realizable. The preceding analysis for physical moment realizability follows from the early work of Hamburger [20,45] and is equivalent to the now classical Hamburger moment problem.

7.2 Physical realizability of 5-moment distribution functions

By dimensional analysis and the requirement of Galilean invariance, it can be shown that, without loss of generality, a 5-moment distribution function can be non-dimensionalized such that $\rho = 1$, $u = 0$ and $p = 1$. The questions of realizability can therefore be explored on a non-dimensional $q^\star$–$r^\star$ plane with

$$q^\star = \frac{1}{\rho}\left(\frac{\rho}{p}\right)^{\frac{3}{2}} q \quad \text{and} \quad r^\star = \frac{1}{\rho}\left(\frac{\rho}{p}\right)^{2} r \tag{55}$$

Once this non-dimensionalization has been carried out, the matrix $\bar{\mathbf{Y}}$ of Eq. (54) that will show the region of physical realizability for the five moments considered in the above closure can be generated using the velocity weights $\mathbf{M} = [1, v, v^2]$ and can be written as

$$\bar{\mathbf{Y}} = \begin{bmatrix} 1 & 0 & 1 \\ 0 & 1 & q^\star \\ 1 & q^\star & r^\star \end{bmatrix}. \tag{56}$$

This matrix is positive definite whenever $r^\star \geq 1 + (q^\star)^2$. These states are therefore physically possible. This is not to say that all points on this plane are realizable by a distribution function of the form given in Eq. (46) but that for any state that $r^\star \geq 1 + (q^\star)^2$, there exists *some* corresponding positive-valued distribution function.

7.3 Realizability of maximum-entropy distribution functions

As has been shown by Junk, there do exist moment states that satisfy the constraints on physical realizability but for which the entropy-maximization problem does not have a solution [i.e., there is no corresponding distribution function of the form given in Eq. (46)] [29,30]. In these situations, the distribution function that has the maximum entropy while being consistent with the moments cannot be said to exist.

Following the analysis of Junk, the physical region for which the entropy-maximization problem cannot be solved is found to be the line on which $q^\star = 0$ and $r^\star > 3$. This last constraint is particularly troubling, as the point at the end of this line, $q^\star = 0$ and $r^\star = 3$ is the point that corresponds to local thermodynamic equilibrium. The physically realizable region and line along which no maximum-entropy distribution exists is depicted in Fig. 1.

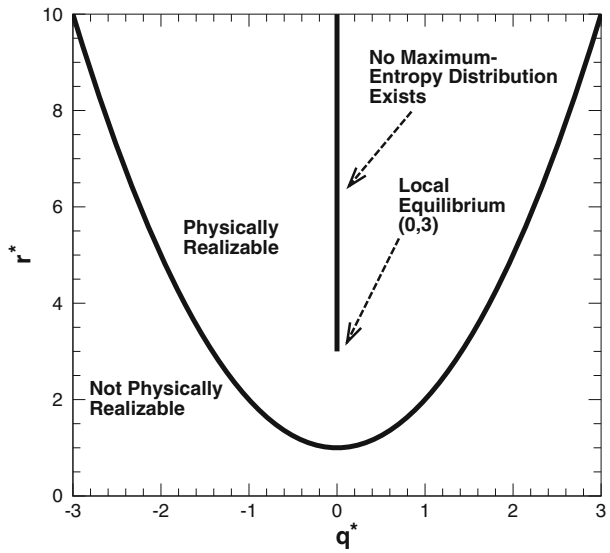

Fig. 1 Region of physical realizability and realizability of maximum-entropy distribution function for the one-dimensional 5-moment system

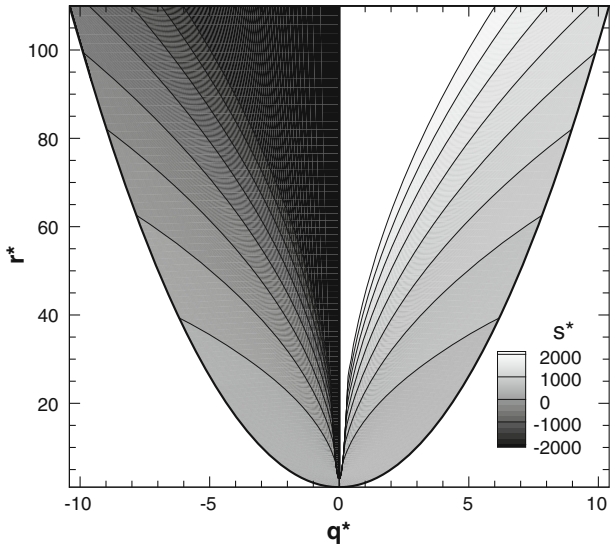

Fig. 2 Non-dimensionalized closing flux $s^\star$ for the one-dimensional, 5-moment, maximum-entropy closure

This issue of non-solvability of the entropy-maximization problem is related to the inability to satisfy simultaneously all of the restrictive conditions on the closure coefficients, $\boldsymbol{\alpha}$, which ensure that the polynomial $(\boldsymbol{\alpha})^{\mathrm{T}}\mathbf{V}$ in Eq. (8) decreases towards negative infinity in all directions as $|v_i|$ becomes large. More devastating still, for all higher-order moment closures, the equilibrium state lies on the boundary in moment space separating regions in which the entropy-maximization problem can be solved and regions in which a solution is not possible [30]. This seems to leave little hope that numerical solutions to moment-closure problems can be computed for any practical situations.

Investigation of the behaviour of the non-dimensional closing flux, $s^\star$, as a function of $q^\star$ and $r^\star$ shows the practical nature of the problem of realizability for this 5-moment system. The closure is not defined on the line extending upward from the point (0, 3). It can be seen in Fig. 2 that as this line is approached from either the left or the right, the closing flux diverges quickly towards negative or positive infinity, respectively. For practical use of higher-order moment closures, it is not only the mathematical problem of realizability that must be overcome as, even in realizable regions, the flux becomes arbitrarily large and could never be computed using finite-precision arithmetic. This issue could be referred to as a problem of numerical realizability.

8 Realizable distribution functions

One possible technique to avoid issues with non-realizability of maximum-entropy closures that is explored herein is to modify slightly the assumed form of the distribution function. This can be accomplished by adding an additional term or factor, σ, to the exponential of Eq. (8) to yield

$$\mathcal{F} = e^{(\boldsymbol{\alpha}^{\mathrm{T}}\mathbf{V}+\sigma)} = e^{(\boldsymbol{\alpha}^{\mathrm{T}}\mathbf{V})} f_w, \tag{57}$$

where $f_w = e^{\sigma}$. This type of modification to the maximum-entropy moment distribution was first proposed by Au [2] and then later re-considered by Junk [28]. The modification is equivalent to multiplying the distribution function by a factor f_w that can be viewed as a "window" function that attenuates the distribution at high velocities, thus ensuring the distribution remains finite. In general, σ is a velocity-dependent term that must be chosen such that it approaches negative infinity more quickly than the polynomial, $\boldsymbol{\alpha}^{\mathrm{T}}\mathbf{V}$, can approach positive infinity as $|v_i|$ becomes large in any direction. This allows the closure to remain valid for all physically realizable sets of velocity moments.

In the case that σ is not a function of the closure coefficients, proof of hyperbolicity as described in Sect. 3 remains valid and the hyperbolic properties of the moment closure are retained. A simple example where this is true is to take $\sigma = -b|v_i|^n$ where b is a positive real value and n is an even integer larger than the highest power of the velocity weights in $\mathbf{V}$. In this case, $\partial\sigma/\partial\boldsymbol{\alpha} = 0$ and the proof of hyperbolicity remains entirely unaltered. Unfortunately, for velocity-weight vectors in the Levermore hierarchy, the closure is no longer

Galilean invariant for this choice of σ. Taking $\sigma = -b|c_i|^n$ leads to a Galilean-invariant closure; however, in this case, $\partial\sigma/\partial\boldsymbol{\alpha} \neq 0$ and hyperbolicity of the closure is not assured. This is because it is no longer possible to ensure in a general manner that $h_{\boldsymbol{\alpha}\boldsymbol{\alpha}}$ is symmetric positive definite.

In practice, it would seem prudent to define σ to be a function of the local solution so as to ensure Galilean invariance of the closure. Moreover, it has been found that it is also desirable to have the effective width of the window function, σ, be dependent on the solution so as to match the standard deviation of the unmodified distribution in some fashion and thereby result in a more appropriate windowing function. In the current work, the modification to the maximum-entropy distribution is chosen to have the form

$$\sigma = -b\left(\frac{\rho}{p}\right)^{\frac{L+2}{2}} |c_i|^{L+2}, \tag{58}$$

where L is the highest exponent of the velocity weights used in the moment closure and b is some specified positive number. This form for σ clearly makes strict proof of hyperbolicity elusive; however, numerical experiments suggest that the resulting moment equations are well behaved and remain hyperbolic for a wide range of flow conditions.

One cause for concern with this proposed approach may be its treatment of equilibrium conditions as the modified-distribution function no longer contains the Maxwellian. Nevertheless, under equilibrium conditions, the moments of the modified-distribution function used in the closure are in full agreement with those of the Maxwellian up to one order higher than the order of the closure provided that the velocity weights of the Levermore hierarchy are used. In addition, all odd-order random-velocity moments of the modified assumed form for the distribution function vanish and are equal to those of the Maxwellian under equilibrium conditions.

It should be noted that the introduction of the window function no longer requires the strict use of the velocity weights, $\mathbf{V}$, proposed by Levermore [32] as the window function will ensure that the distribution function remains finite regardless of the velocity weights. Other choices are therefore possible for the velocity moments of the closure while still remaining both realizable and hyperbolic [28].

8.1 Alternate remedies for non-realizability

Recently, Schneider [22,49] has proposed an alternate approach to dealing with the realizability of maximum-entropy closures. He proposes appropriately relaxing some of the equality constraints on the moments in the entropy minimization procedure when defining the maximum-entropy distribution. This leads to a maximum-entropy solution; however, it is one that does not satisfy the full set of predicted moments (only those that can be satisfied and represented by the maximum-entropy distribution). Unfortunately, this modification results in the entropy function loosing strict convexity at the moments that are not realizable under all of the equality constraints. Hauck et al. [22] have subsequently carried out a thorough mathematical analysis of this alternate approach to modifying maximum-entropy closures.

Mathematically, this approach does preserve hyperbolicity while leading to universally realizable closures. However, there remain practical issues that are not resolved by Schneider's solution. The new closure is modified only in the area where the traditional closure is non-realizable; all other regions are unaltered. Referring to Fig. 2, it is clear that even in regions where the maximum-entropy distribution function exists, there are areas where practical computation of the closing flux will be problematic. In fact, the closing flux still approaches infinity as the problematic line is approached, and there are regions arbitrarily close to equilibrium where the closing flux is arbitrarily large. This means that issues still remain for any solution procedure that makes use of finite-precision arithmetic as numerical overflow can certainly occur.

8.2 Application to one-dimensional 5-moment system

The application of the windowing technique shown above is now considered for the one-dimensional 5-moment system. The resulting distribution function is

$$\mathcal{F} = e^{\alpha_0+\alpha_1 c+\alpha_2 c^2+\alpha_3 c^3+\alpha_4 c^4-b(\rho/p)^3 c^6} = e^{\alpha_0+\alpha_1 c+\alpha_2 c^2+\alpha_3 c^3+\alpha_4 c^4} e^{-b(\rho/p)^3 c^6}, \tag{59}$$

where $f_w = e^{-b(\rho/p)^3 c^6}$ is the window function. The parameter, b, can be adjusted to modify the effective width of the window. For $b = 0$, the maximum-entropy closure is recovered. Figure 3 shows the numerical

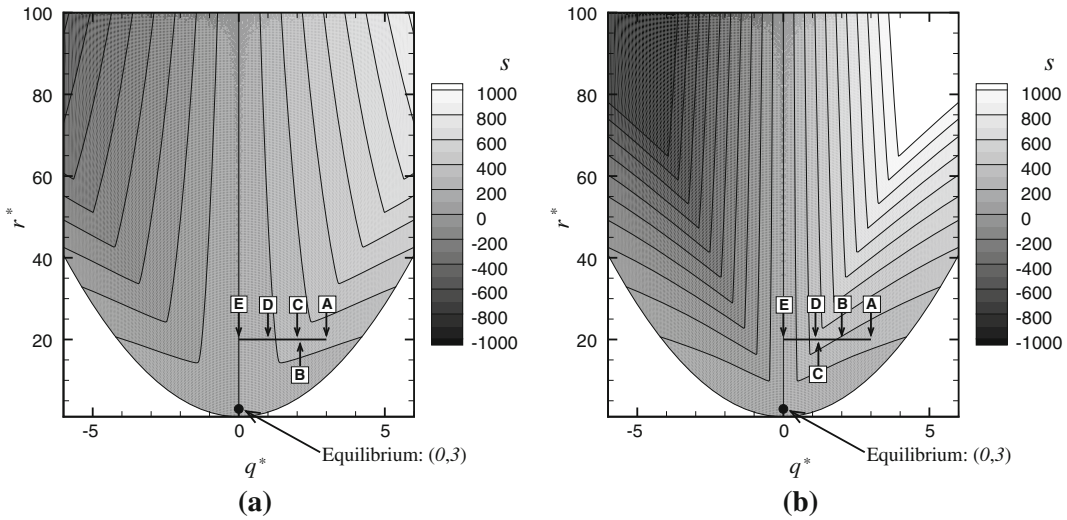

Fig. 3 Predicted fifth-order non-dimensional random-velocity moment, $s^\star$, as a function of $q^\star$ and $r^\star$ for the 5-moment one-dimensional realizable moment closure with **a** $b = 10^{-4}$; and **b** $b = 10^{-5}$

computation of $s^\star$ as predicted by the new closure for a wide range of physically realizable situations for $b = 10^{-4}$ and $b = 10^{-5}$. For these two values of b, the modified realizable distribution function fully spans the region in $q^\star$–$r^\star$ space of all physically realizable moments and values for $s^\star$ are computable. In fact, the proposed closure is technically realizable for all positive non-zero values of b; however, in practice, b must be large enough that it ensures that the moments of the distribution function remain numerically computable by finite-precision arithmetic. It is interesting to note that it appears that $s^\star$ may not be a smooth function of $q^\star$ and $r^\star$ as indicated by the sharp changes in the contour lines.

From Fig. 3, it is evident that the modification to the maximum-entropy distribution function has resulted in a moment closure that covers the whole realizable moment space; however, formal proof of global hyperbolicity is not possible in this case. Hyperbolicity of the proposed closure is instead investigated numerically. If the flux Jacobians are computed numerically using a second-order accurate centred finite-difference technique, eigenvalues of the Jacobians can then be computed numerically. The system of moment equations is deemed hyperbolic whenever the eigenvalues are real. Figure 4 shows the largest imaginary part of the computed eigenvalues as a function of $q^\star$ and $r^\star$ for the normalized distribution function, again for the cases where $b = 10^{-4}$ and $b = 10^{-5}$. The computed eigenvalues do not remain real, and hence, the system appears not to be globally hyperbolic. Fortunately, as b decreases, the region of hyperbolicity expands greatly. It should be obvious that for $b = 0$, the closure will be hyperbolic but not realizable and as b is increased, the closure is now realizable but the region of hyperbolicity is reduced and does not span the full range of realizable moments. This points to a trade-off in the selection of the realizability parameter, b: it must be non-zero and large enough so that all moments are numerically integrable (numerically realizable) but sufficiently small so that the closure remains hyperbolic for the non-equilibrium flow conditions of interest.

In order to gain a feel for the degree of non-equilibrium behaviour that is contained in the hyperbolic region, the orbits of moments describing the structure of shock waves with shock Mach numbers of 2, 4 and 8 as predicted by a high-resolution numerical solution of the BGK kinetic equation [Eq. (18)] are shown in both Fig. 4a, b. The orbit corresponding to a shock with an upstream Mach number of 2 is quite small as compared to that of the stronger shocks. It can be observed that, if b is taken to be 10^{-5}, even the relatively high shock-Mach-number case remains in the hyperbolic region. The appearance of complex eigenvalues along the lines across which $s^\star$ exhibits very non-smooth behaviour as a function of $q^\star$ and $r^\star$ is most likely due to the unsuitability of finite differences across this line. The hyperbolic nature of the closure and its moment equations is difficult to evaluate on this line; however, in practice, no issues were observed.

The origin of the apparent non-smooth behaviour of $s^\star$ can be understood through an examination of the underlying distribution function. Figure 5 shows the natural logarithm of the modified, realizable, 5-moment distribution functions for various values of $q^\star$ with $r^\star = 20$ and $b = 10^{-4}$ and $b = 10^{-5}$ (the exact locations investigated are shown on Fig. 3). It can be seen that, when $q^\star = 3$ (location A), the distribution function is bimodal with most particles having low speeds and a small portion or parcel with higher velocity. As $q^\star$ is

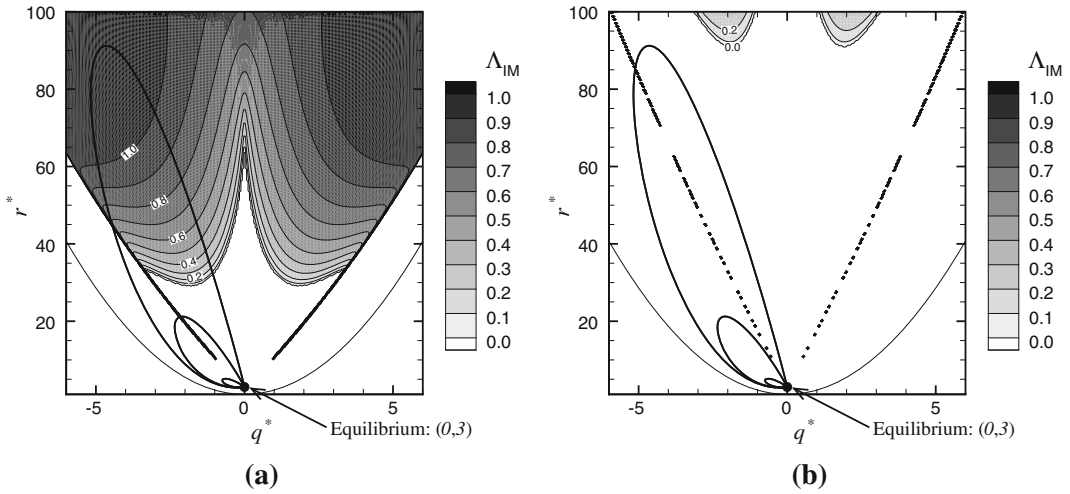

Fig. 4 Largest imaginary part of the numerically determined eigenvalues of flux Jacobian for the modified, realizable, 5-moment moment closure with **a** $b = 10^{-4}$, and **b** $b = 10^{-5}$. The orbits of velocity moments corresponding the transition and internal structure for stationary shock-wave solutions with shock Mach numbers of Ma = 2, Ma = 4, and Ma = 8 are also shown with the larger orbits corresponding to the higher shock Mach numbers

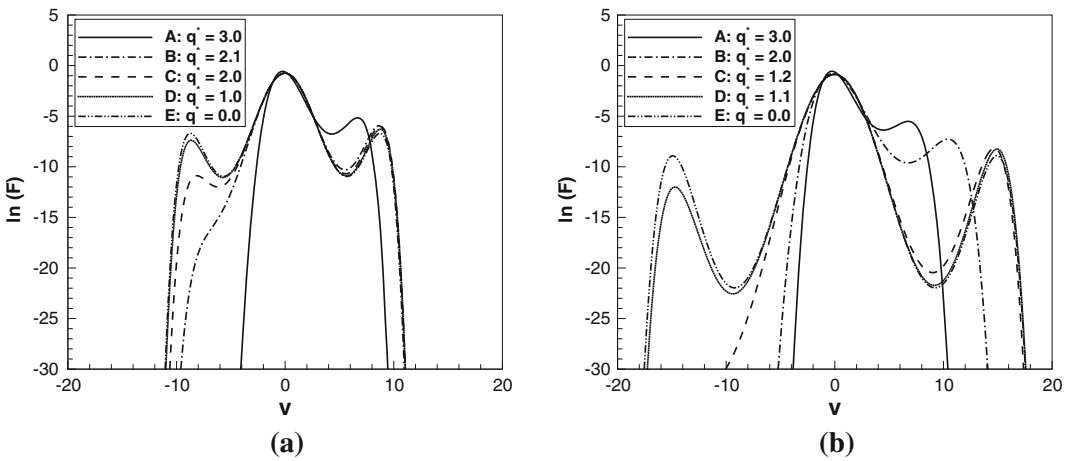

Fig. 5 Natural logarithm of modified, realizable, 5-moment moment closure with **a** $b = 10^{-4}$, and **b** $b = 10^{-5}$ for $r^\star = 20$ at various values of $q^\star$. The exact locations are also shown on Fig. 3

reduced, this small parcel of faster-moving particles begins to reduce in size (i.e., the number of high-speed particles is reduced) but, at the same time, the speed of these particles is increased. In the unmodified maximum-entropy case, the number of particles in this high-speed packet approaches zero as the velocity of the particles in the parcel approaches positive infinity [31]. For the new modified realizable closure, the tendency for the velocities of the particles in the high-speed parcel to increase is eventually overwhelmed by the windowing function and a maximum in achieved. At this point, another small parcel of particles having high negative velocities quickly appears. This appearance of the latter is what leads to the very sharp changes in the distributions of $s^\star$. When $q^\star = 0$ (location E) the packets of both positive- and negative-moving particles now have the same size and speed (i.e., the number of particles in each oppositely moving high-speed parcel is the same) yielding a symmetric distribution function.

Even though the distribution function is now realizable and it appears to have a large enough region of hyperbolicity for many problems, it remains to be seen how well solutions of the new moment system agree with solutions of the higher-dimensional kinetic equation. As with all moment closures, there is no formal estimate on the error for the closing fluxes, and the predictive validity of the system must be evaluated through numerical experimentation. This is the topic of the next subsections.

8.3 Godunov-type finite-volume scheme

As a preliminary investigation of the predictive capability offered by the proposed higher-order realizable hyperbolic moment equations, a numerical-solution procedure has been constructed for the one-dimensional moment system described above. The moment equations are solved using a Godunov-type finite-volume scheme. The HLL [21] approximate Riemann solver is used to evaluate inter-cellular fluxes, for which estimates for the maximum and minimum wave speeds are based on the numerical evaluation of the eigenvalues of an approximate flux Jacobian for the moment closure. Higher-order accuracy is achieved through piecewise limited linear reconstruction and a point-implicit predictor-corrector time-marching scheme that treats the hyperbolic terms explicitly and the collisional terms implicitly is used to advance the solution [35]. The fully discrete finite-volume formulation applied to the ith cell is given by

$$\tilde{\mathbf{U}}_i^{n+1} = \mathbf{U}_i^n + \frac{\Delta t}{\Delta x}\left(\mathbf{F}_{i-\frac{1}{2}} - \mathbf{F}_{i+\frac{1}{2}}\right) + \Delta t\, \tilde{\mathbf{S}}_i^{n+1}\,, \tag{60}$$

$$\mathbf{U}_i^{n+1} = \mathbf{U}_i^n + \frac{\Delta t}{2\Delta x}\left(\mathbf{F}_{i-\frac{1}{2}} - \mathbf{F}_{i+\frac{1}{2}} + \tilde{\mathbf{F}}_{i-\frac{1}{2}} - \tilde{\mathbf{F}}_{i+\frac{1}{2}}\right) + \Delta t\left(\frac{\mathbf{S}_i^n + \mathbf{S}_i^{n+1}}{2}\right), \tag{61}$$

where $\mathbf{U}_i$ is the conserved solution vector for the ith cell, $\mathbf{F}_{i\pm\frac{1}{2}}$ is the flux dyad evaluated at the cell interface, and $\mathbf{S}_i$ is the effect of the source vector on the cell-average state. The superscript n is the index for the time step of size Δt. This time-marching formulation allows the maximum time step to be determined by the usual CFL condition rather than being governed by the relaxation-time scale of the stiff source terms.

As stated earlier, for the 5-moment closure, there is no explicit conversion from conserved moments, $\mathbf{U}$, to the closure coefficients, $\boldsymbol{\alpha}$. The evaluation of the highest-order flux requires that all of the coefficients be known at each time step. These coefficients can be determined by finding the extremum of Eq. (16) with the modified-distribution function used to define a modified density potential. This leads to a minimization problem given by

$$\min_{\boldsymbol{\alpha}} \left[\langle \exp(\boldsymbol{\alpha}^{\mathrm{T}}\mathbf{V} + \sigma)\rangle - \boldsymbol{\alpha}^{\mathrm{T}}\mathbf{U}\right]. \tag{62}$$

By making the term σ dependent on the "target" moments, this function remains convex. The minimization problem can therefore be solved using an approximate Newton's method. In some cases, it is possible for the computed update from Newton's method to move the vector $\boldsymbol{\alpha}$ to a location where numerical integration of the moments is not possible. When this happens, a simple back-tracking technique is used to step back into a computable region of moment space.

8.4 Numerical calculations of stationary shocks

Predictions of the structure of stationary shocks for the one-dimensional gas obtained by solving the 5-moment version of the physically realizable moment equations are now considered. The numerical results are shown in Fig. 6 and compared with numerical solutions to the equivalent Navier–Stokes-like equations given previously for a range of shock Mach numbers. Due to the expense of solving the re-synchronization problem, it was only affordable with the current methodology to use a grid in physical space comprising 1,000 volumes; however, this resolution is sufficient for the evaluation purposes here. High-resolution numerical solutions of the one-dimensional BGK kinetic equation for this one-dimensional gas are also depicted for comparison. The discrete-velocity method of Mieussens [39] is used to obtain the numerical solution of the one-dimensional kinetic equation with a region of velocity space stretching from $-5{,}000$ to $5{,}000\,\mathrm{m/s}$ discretized into 500 equally spaced points for the cases with a shock Mach number of 2 and 4 and from $-10{,}000$ to $10{,}000\,\mathrm{m/s}$ discretized into 1,000 equally spaced points for the case of the shock with a Mach number of 8. This expanded region of velocity space was needed for the higher-Mach-number case in order to properly represent the distribution function of the high-temperature gas after the shock wave. It can plainly be observed that the results for the 5-moment system are in much better agreement with the BGK solution than those of the Navier–Stokes-like solution. As with all hyperbolic systems, discontinuities appears in the moment solution when the incoming flow speed exceeds the maximum wavespeed in the system. In this case, however, the size of the jump is very

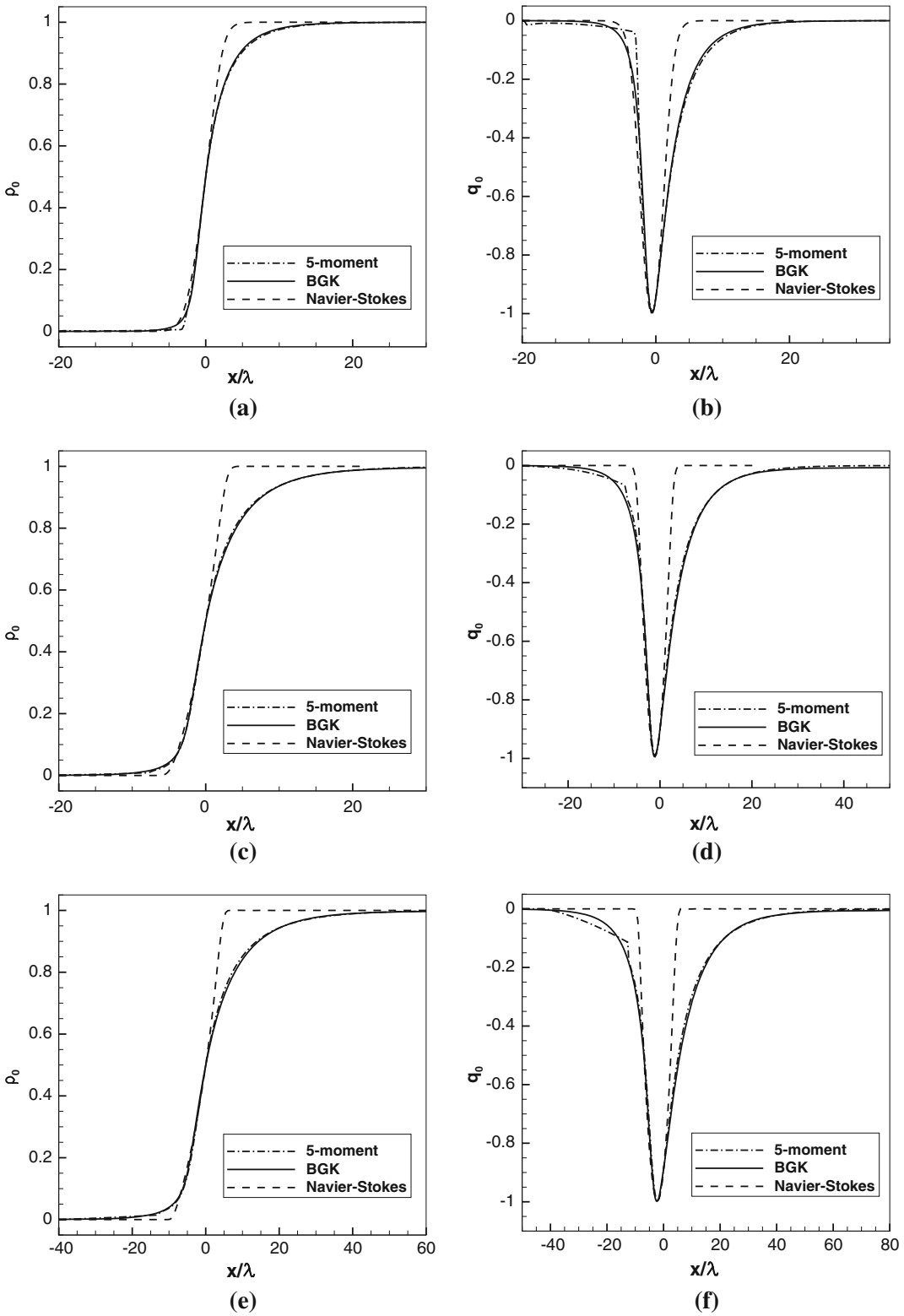

Fig. 6 Predicted normalized density and heat transfer through a stationary shock wave for a one-dimensional gas as determined using the modified, realizable, 5-moment closure with $b = 10^{-5}$. The predicted shock structure is compared to results obtained by the direct numerical solution of the BGK kinetic equation and Navier–Stokes-like equations for a range of shock Mach numbers, **a**, **b** Ma = 2, **c**, **d** Ma = 4, and **e**, **f** Ma = 8

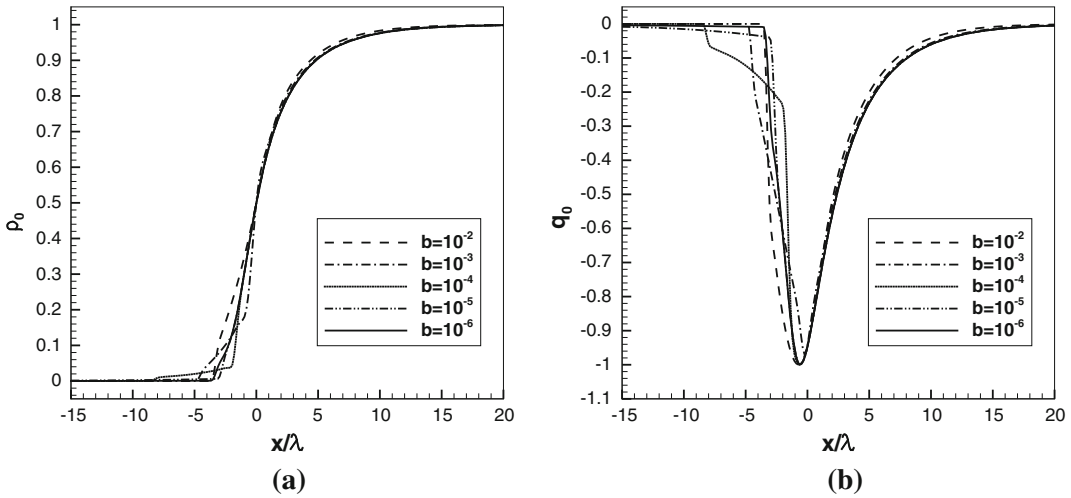

Fig. 7 Comparison of density and heat-transfer profiles through a shock wave with a Mach number of 2 computed using the modified, realizable, 5-moment closure with varying values of the coefficient, b

small. This is in contrast to many other moment-closure predictions of shock structure where the size of the discontinuity tends to grow with the shock Mach number and quickly dominates the profile.

The effect that varying the parameter b has on the predicted shock structure for a shock wave with a Mach number of 2 is demonstrated in Fig. 7. It can be seen that when b is larger than 10^{-5}, significant variations in the front half of the shock structure are observed. Nevertheless, the solutions with $b = 10^{-5}$ and $b = 10^{-6}$ are quite similar. For higher Mach numbers, the solutions leave the region of hyperbolicity for larger values of b. For the case with a Mach number of 8, even using $b = 10^{-4}$ leads to large instabilities and a steady solution cannot be computed. Also at this higher Mach number, re-synchronization of the moments and closure coefficients becomes much more difficult for the case with $b = 10^{-6}$. A value of $b = 10^{-5}$ was effective for all cases considered in this paper.

At this point, it is interesting to compare the velocity distribution function predicted by the solution of the BGK equation to those predicted by the 5-moment maximum-entropy-based method. Three points within the shock wave with a Mach number of 8 are considered. Firstly, the point at $x/\lambda = -35$ is investigated in Fig. 8a. This point is immediately after the small sub shock in the moment-closure solution. As can be seen in the figure, the predicted distribution function for the 5-moment computation is in good agreement with that predicted during the BGK calculation. Figure 8b shows the same velocity distributions at the point $x/\lambda = 0$ (the point where the density is halfway between the upstream and downstream values). In this figure, it is obvious that the distribution functions are very different. What is most significant, however, is that the lower-order moments of both distribution functions (the ones used in the moment calculation) are in close agreement. This emphasizes the fact that, where moment methods are concerned, accurate representation of the true distribution function is not necessarily the goal. It is sufficient to chose distribution functions that will accurately predict closing fluxes for known input moments. In Fig. 8c, at $x/\lambda = 20$, it can be seen that the maximum-entropy-based distribution function is again in good agreement with the kinetic solution. Figure 8d shows the normalized closing moment, $U_5 = \langle mv^5\mathcal{F}\rangle$, for the 5-moment method as compared to the BGK solution. It can be seen that there is good agreement throughout the shock profile.

8.5 Numerical calculations of Riemann problem

In order to explore further the behaviour of the modified 5-moment closure across a range of Knudsen numbers, a Riemann initial-value problem is considered. The case of interest consists of a two-state initial condition with a pressure ratio of 2.5 and a density ratio of 2. Three different situations were examined corresponding to Knudsen numbers of 2.3×10^{-5}, 2.3×10^{-2} and 23, thus spanning the continuum, transition and free-molecular flow regimes. A computational grid of 300 volumes is used. The resulting solutions are shown in Fig. 9. Here, the 5-moment system is compared to the 3-moment closure (which is equivalent to the Euler equations for a one-dimensional gas), high-resolution numerical solutions of the BGK kinetic equation and

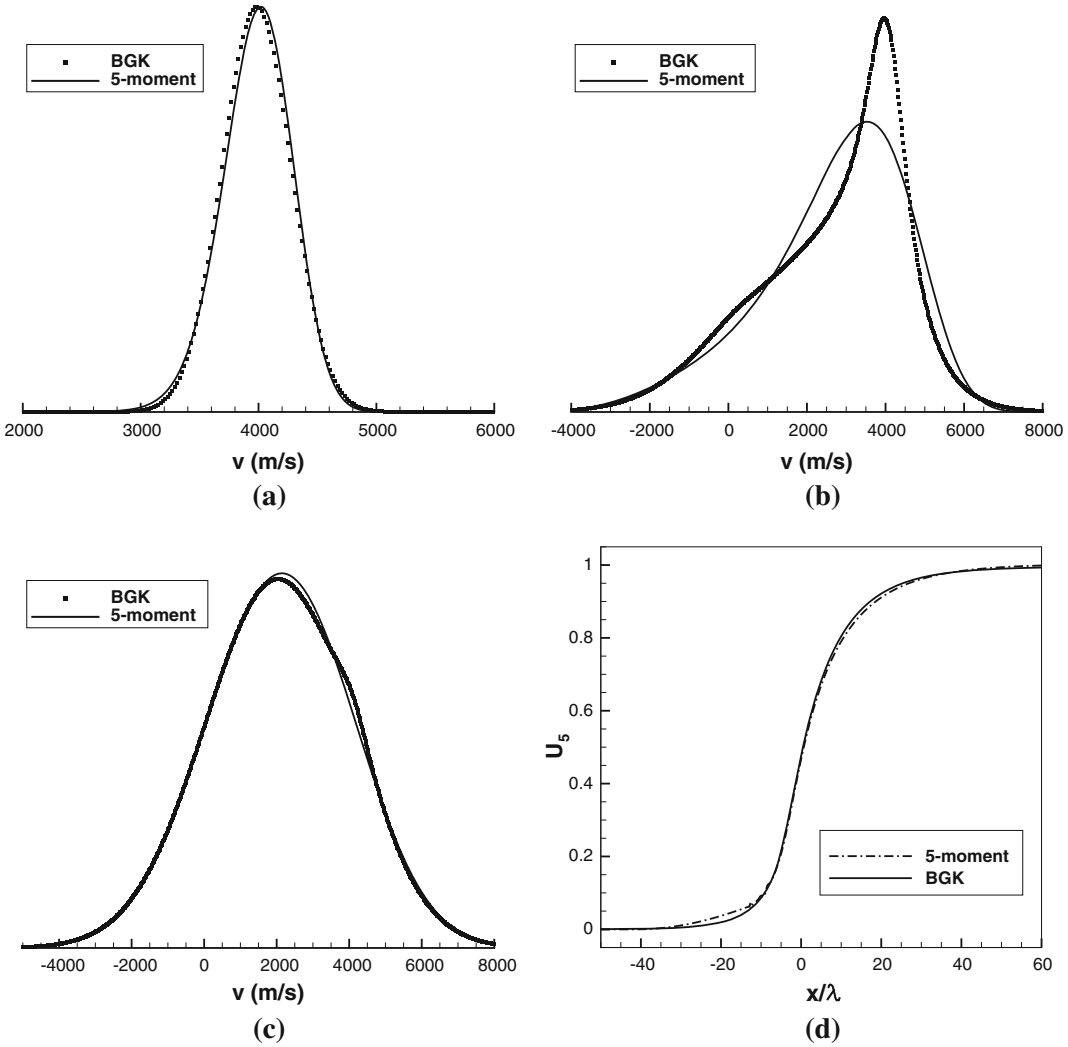

Fig. 8 Velocity PDFs predicted by high-resolution solution of the one-dimensional BGK equation for a shock wave with and upstream Mach number of 8 compared to velocity PDFs corresponding to the numerical solution of the 5-moment realizable moment closure with $b = 10^{-5}$. Sample locations are **a** $x/\lambda = -35$, **b** $x/\lambda = 0$, **c** $x/\lambda = 20$. The normalized closing moment, $U_5 = \langle mv^5\mathcal{F}\rangle$, for the 5-moment method as compared to the BGK solution is shown in **d**

numerical solution of the equivalent Navier–Stokes-like equations. All of which were described above. Again, the discrete-velocity method of Mieussens [39] is used to obtain the kinetic solutions now with a resolution of 200 points stretching from $-2{,}000$ to $2{,}000$ m/s.

It can be seen in Fig. 9a, b that, in the continuum regime, all three non-equilibrium solutions treatments are in close agreement with the equivalent Euler-like equations for this one-dimensional gas. On this scale of interest, the regions of the flow that are not in local thermodynamic equilibrium are much smaller than the domain of interest and are generally not resolved.

Figure 9c and d depicts the numerical results for the transition regime, lying somewhere between continuum and free-molecular results. In this regime, the 3-moment model, which can only correctly account for flows in thermodynamic equilibrium, gives an identical solution, although on a different scale, to that found for the continuum regime. The non-equilibrium solutions of the 5-moment model, Navier–Stokes equations and BGK equation on this scale are all still quite similar to each other in this case but are now quite distinct from the equilibrium or equivalent Euler-like result. For the non-equilibrium solutions, the wave structures that appear as discrete near discontinuities in the continuum situation are still identifiable but are now quite diffuse and approach one another such that they interact, yielding a solution with a smooth transition between the two constant initial states at either end of the solution domain.

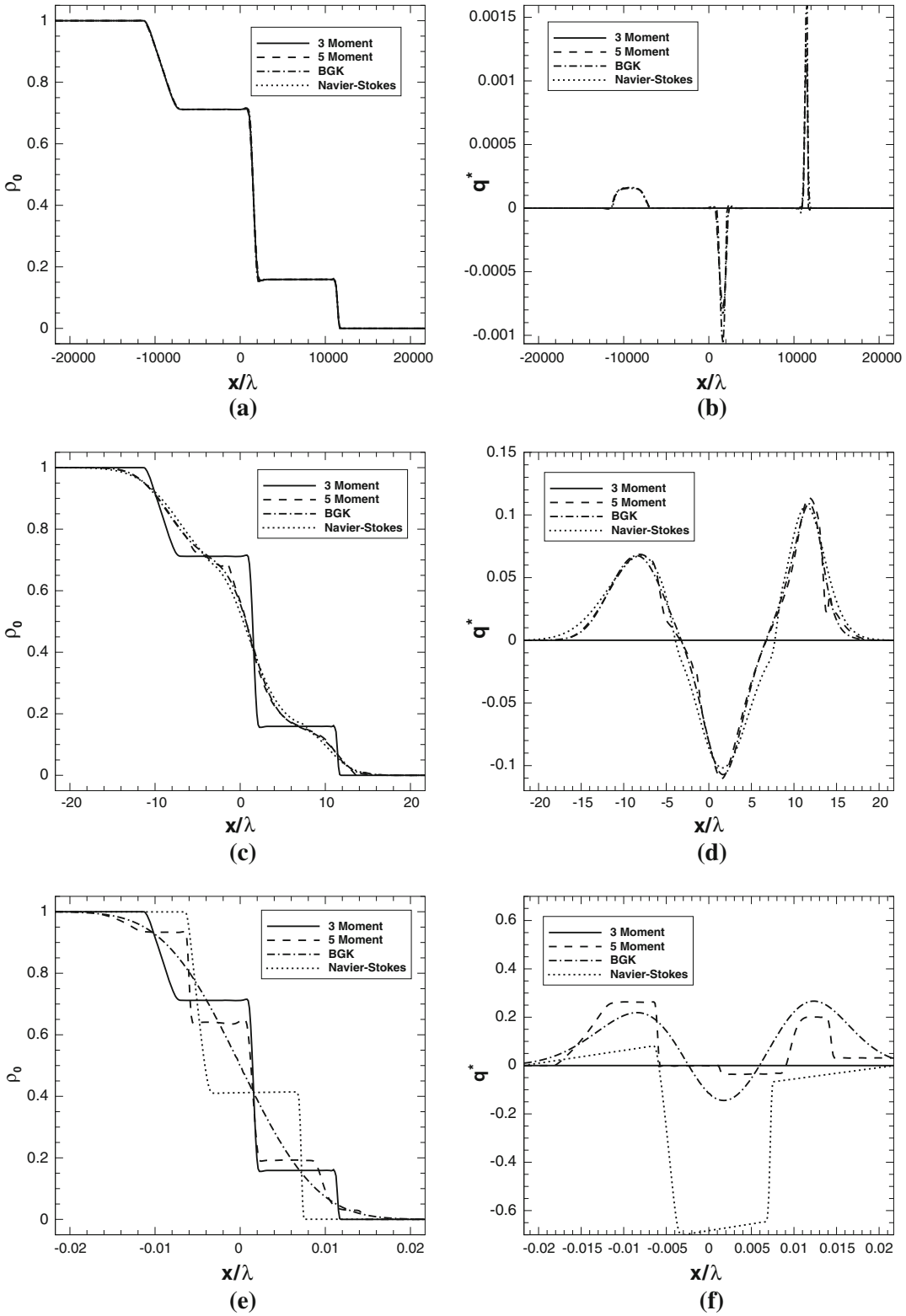

Fig. 9 Predicted normalized density and heat flux for the Riemann initial-value problem as determined using the modified, realizable, 5-moment closure with $b = 10^{-5}$ as compared to the equilibrium 3-moment closure, the kinetic equation, and the Navier–Stokes-like solutions for a range of Knudsen numbers: **a**, **b** Kn $= 2.3 \times 10^{-5}$, **c**, **d** Kn $= 2.3 \times 10^{-2}$ and **e**, **f** Kn $= 23$

The free-molecular results for the Riemann initial-value problem are given in Fig. 9e, f. For this case, the 3-moment model again yields results that are the same as those for the continuum flow solution. For the modified 5-moment model, due to infrequent inter-particle collisions, the terms associated with the collision operator have now become so insignificant that the moment closure essentially behaves as a purely hyperbolic system without relaxation. It yields a solution with five distinct waves separated by essentially constant solution states. This non-equilibrium result is in contrast to the BGK kinetic equation solution, which consists of a single smooth transition between the two constant initial states, with no clearly identifiable wave structure. The agreement between 5-moment-closure solution and the exact or BGK kinetic solution is certainly not very good in this case, indicating that, while it is still possible to obtain solutions, there is an upper bound on the Knudsen number for which the 5-moment model remains physically valid. Higher-order moment closures would be needed to improve on this result. For this highly rarefied case, the speed with which significant heat-transfer effects are carried in the Navier–Stokes case is over predicted and is so high that any temperature differences are smoothed out extremely rapidly. These thermal effects move so quickly relative to the hyperbolic components of the equations that they impact the boundary of the computational domain almost immediately, and therefore, boundary conditions play an important role; in this case, a zero-derivative Neumann boundary condition was used for all variables. Regardless of which boundary condition is used, the speed at which temperature differences are diffused away leads the Navier–Stokes-like equations to predict solutions that approach the solution to the isothermal Euler solution. This is why a two-wave solution is predicted in this case.

9 Closed-form approximation to a maximum-entropy moment closure

As stated earlier, one of the major stumbling blocks to the adoption of maximum-entropy-based moment closures is the lack of a closed-form expression for closing moment fluxes. It will now be shown that a simple surface fit can provide an adequate approximation to the true maximum-entropy 5-moment closure above, Eqs. (47)–(51). By using a fit in this manner, the complexity and expense of moment and distribution function resynchronization can be avoided. Numerical-solution costs are therefore reduced by orders of magnitude. Moreover, and somewhat serendipitously, this fit will also avoid the problem of non-realizability of the true maximum-entropy closure.

Firstly, it should be noted that along the line defining the envelope of the region of physical realizability, $r^\star = 1 + (q^\star)^2$, the distribution function is comprised of two delta functions. On this line, the closing relationship can be easily found analytically and is $s^\star = (q^\star)^3 + 2q^\star$. Next, realizing that the region of realizability is parabolic, it seems sensible to parametrize this space using a parabolic transformation of the form given by

$$r^\star = \frac{2(q^\star)^2}{\sigma} + 3 - \sigma \quad \text{with} \quad 0 \le \sigma \le 2. \tag{63}$$

For this mapping, lines of constant σ are parabolas and σ is the distance down from local equilibrium, $r^\star = 3$, that these lines intersect the $r^\star$ axis. These parabolas have curvatures that increase from $\sigma = 2$, where the parabola coincides with the limit of physical realizability, to $\sigma = 0$ where the parabola collapses to the line $q^\star = 0$ and $r^\star \ge 3$, thus covering the entire realizable region.

It was found through numerical experimentation that along the lines of constant σ, the moment $s^\star$ can be well approximated by a cubic function of $q^\star$ as $s^\star = p_3(\sigma)(q^\star)^3 + p_1(\sigma)q^\star$. The functions $p_3(\sigma)$ and $p_1(\sigma)$ must be fit by first numerically finding finite-difference approximations to these derivatives along the line $q^\star = 0$ and $1 \le r^\star \le 3$. These data points are then fit using standard fitting software; it has been found that these functions are well approximated as

$$p_1 = a_1 + b_1\sigma + c_1\sigma^2 + d_1\sigma^3 + e_1\sigma^4 + f_1\sigma^5 + g_1\sigma^6, \tag{64}$$

with

$$\begin{array}{ll} a_1 = 9.9679007422678190 & e_1 = 4.3920303941514343 \\ b_1 = -9.234367231975216 & f_1 = -1.452821303578764 \\ c_1 = 8.2142492688404296 & g_1 = 0.2006200057926356 \\ d_1 = -7.372320367163680 & \end{array},$$

and

$$p_3 = \frac{a_3 + b_3\sigma + c_3\sigma^2 + d_3\sigma^3}{1 + e_3\sigma + f_3\sigma^2 + g_3\sigma^3}, \tag{65}$$

with

$$\begin{aligned} a_3 &= -20840.93761193234 & e_3 &= -1077.797102997202 \\ b_3 &= 7937.3772948278038 & f_3 &= -3072.303291055466 \\ c_3 &= 405.05250560053173 & g_3 &= 1056.0890741355661 \\ d_3 &= -329.3827765656151 \end{aligned} .$$

Having determined the fits above, the closing flux is expressible as a closed-form function of $q^\star$ and $r^\star$.

9.1 Accuracy of fit and hyperbolicity

Figure 10a, b show the non-dimensionalized closing flux, $s^\star$ of the 5-moment maximum-entropy system as well as the surface fit shown above. The relative error is plotted in Fig. 11. It can be seen that away from the line on which the maximum-entropy distribution does not exist and the predicted flux is singular, the fit is quite good. In practice, the fact that the fit does not approximate the singularity well is actually advantageous as the fit transitions smoothly across the $r^\star$ axis and numerical overflow is avoided.

Once again, there is no formal proof of hyperbolicity when this surface fit is used for the closing flux. However, experience gained from numerical calculation of many flows using this fit suggests that non-hyperbolicity does not seem to be an issue for a wide range of conditions.

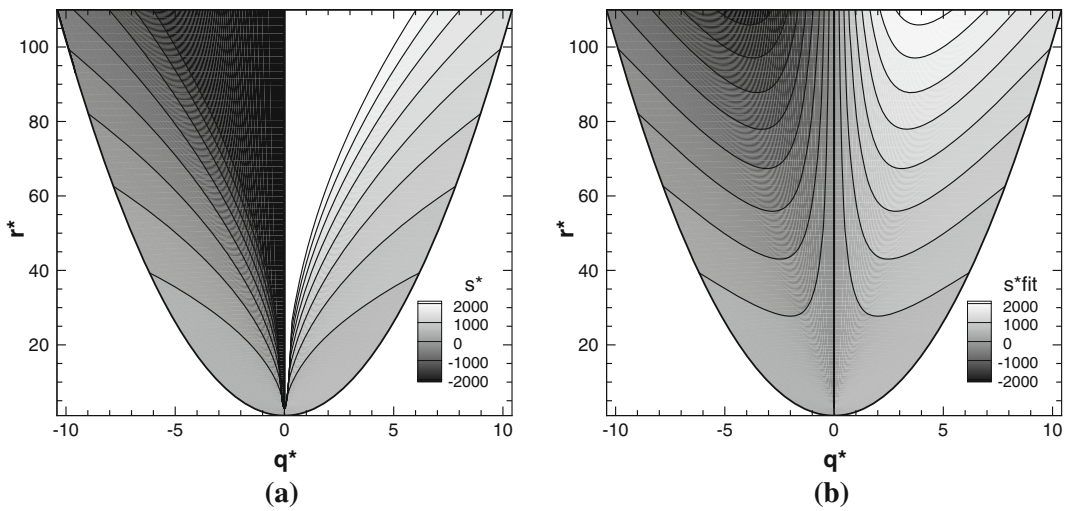

Fig. 10 **a** $s^\star$ predicted by maximum-entropy closure. **b** $s^\star$ predicted by surface fit

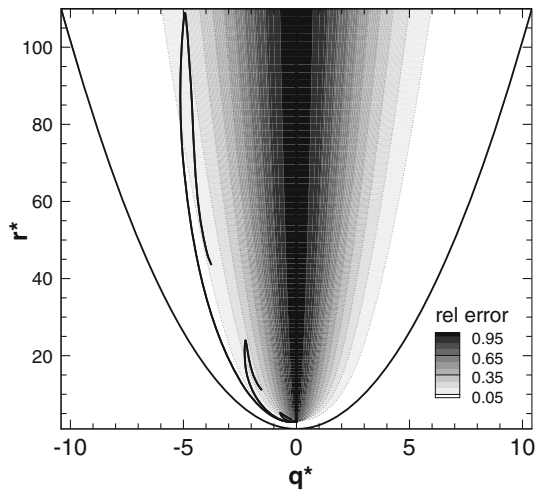

Fig. 11 Relative error between fit and true moment $s^\star$ and orbits for shock waves with Mach numbers 2, 4 and 8

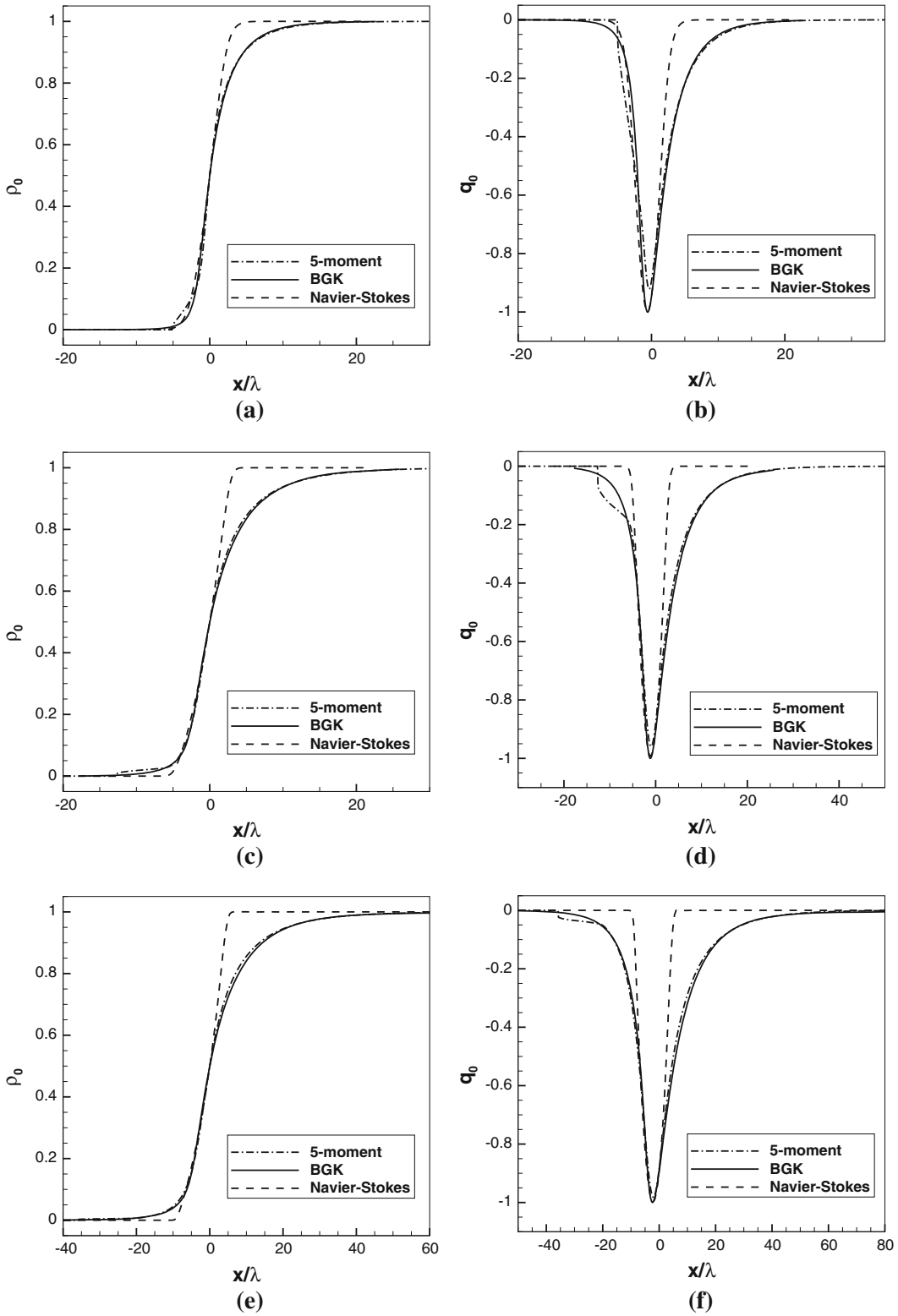

Fig. 12 Predicted normalized density and heat transfer through a stationary shock wave for a one-dimensional gas as determined using a surface fit for the closing flux of the maximum-entropy 5-moment closure. The predicted shock structure is compared to results obtained by the direct numerical solution of the BGK kinetic equation and Navier–Stokes-like equations for a range of shock Mach numbers. **a**, **b** Ma = 2, **c**, **d** Ma = 4, and **e**, **f** Ma = 8

9.2 Numerical calculations of shock structures

As a preliminary investigation into the behaviour of the fitted moment closure, shock waves of Mach numbers 2, 4 and 8 are again considered. Once again, the same Godunov-type finite-volume scheme is used. The costly re-synchronization step is now unnecessary as the closing flux is known as a function of the known moments. A computational mesh with 5,000 volumes can now easily be used to ensure a solution that is entirely grid-converged. Eigenvalues must still be determined in order to use the HLL flux function; these are found numerically using the analytic flux Jacobian.

Comparisons are once again made to high-resolution simulation of the kinetic equation, Eq. (18), with the same relaxation collision operator as was used in the moment equations [5] and with the equivalent Navier–Stokes-like equations for this situation. Figure 12a, c, e show normalized density profiles for shocks with a Mach number of 2, 4 and 8, respectively, while normalized heat transfer is shown in Fig. 12b, d, f.

It can be seen that agreement between the moment equations and the BGK equation is again very good, far better than the Navier–Stokes-like equations. The profiles predicted by the surface fit are very comparable to the profiles predicted by the modified, realizable, 5-moment system of Sect. 8. The same relatively small discontinuities in the shock profile are again present. Figure 11 shows the orbits traced by these shock profiles in the $\hat{q}$–$\hat{r}$ plane. All shocks begin at equilibrium, jump to a non-equilibrium state across the discontinuity and return smoothly to equilibrium. It can be seen that in all cases, the area of largest relative error in the fit is avoided.

9.3 Numerical calculations of Riemann problem

Finally, the 5-moment-closure fit it used for the computation of the Riemann problem of Sect. 8.5. For this case, a computational mesh comprising 3, 000 cells was used. The results are shown in Fig. 13. Once again, solutions are almost identical to those obtained with the modified, realizable, 5-moment closure. The same transition from a three-wave equilibrium solution through a diffuse smooth transition into a 5-wave non-equilibrium solution is observed. The only difference in solution that is noticeable to the eye is in the heat-flux prediction for the free-molecular case (Figs. 9f, 13f). These solutions are obtained in orders of magnitude less time than the previous calculations with the costly re-synchronizations of moments and closure coefficients.

10 Remarks regarding computational cost

The computational expense of the different techniques considered in this chapter varied widely. Although real effort has been made to optimize the solution methods or computer implementations of the techniques, it is felt that some remarks on computational cost are warranted.

The numerical solution of the one-dimensional kinetic equation for most of the problems above was the most expensive by a significant amount. Such computations for a realistic three-dimensional gas would obviously require huge computational resources. For example, if the same resolution in velocity space was used in three space dimensions as was used for the shock-structure calculations above, the solution vector in each cell would have over a hundred million entries. This is clearly not an attractive option.

The prospects for the moment closure based on a realizable distribution function shown above are not much better. A similar curse of dimensionality that afflicts the kinetic method also affects this method. The extension to a three-dimensional gas would require the integration of distribution functions that would then exist in a three-dimensional space. Thus, the computational costs of the moment re-synchronization procedure would appear to be prohibitively expensive.

The surface-fit closure is a much more affordable option. The computations carried out above only required several minutes of computing time. Moreover, the extension of this method to a realistic three-dimensional gas does not need to bring the same devastating cost increase as either the kinetic method or the method based on realizable distribution functions. The simplest three-dimensional equivalent to the maximum-entropy 5-moment system shown above is a 14-moment system. Closing fluxes would therefore have to be fit for a higher-dimensional space, but not higher by orders of magnitude.

The time required for the Navier–Stokes-like computations varied based on the Knudsen number. For low-Knudsen-number cases, computations were very fast and required only a matter of seconds in computing time. However, as the Knudsen number increased and the length scales became relatively smaller, the time-step restriction required for stability of the rather simple explicit calculation procedure adopted here becomes

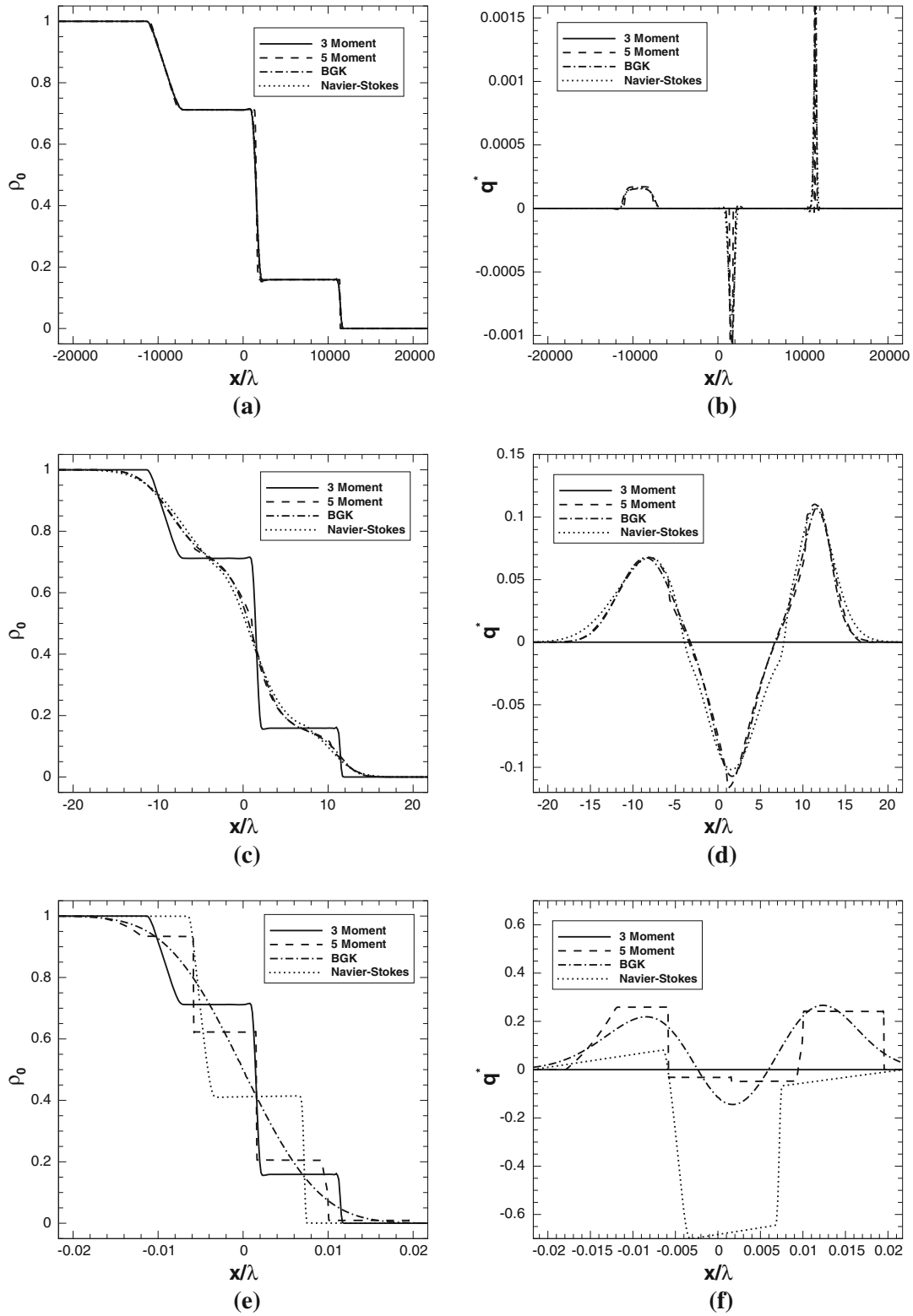

Fig. 13 Predicted normalized density and heat flux for the Riemann initial-value problem as determined using a surface fit for the closing flux of the maximum-entropy 5-moment closure as compared to the equilibrium 3-moment closure, the kinetic equation, and the Navier–Stokes-like solutions for a range of Knudsen numbers: **a**, **b** $\mathrm{Kn} = 2.3 \times 10^{-5}$, **c**, **d** $\mathrm{Kn} = 2.3 \times 10^{-2}$ and **e**, **f** $\mathrm{Kn} = 23$

very restrictive due to the partially elliptic nature of the equations. Use of an implicit solution scheme would alleviate this issue.

Solution of the equilibrium 3-moment equations was obviously far faster than all of the other methods. However, with no treatment for non-equilibrium effects of any sort, the usefulness of these equations for practical problems involving any departure of the solution from equilibrium is very limited.

11 Comparison to other moment closures

Maximum-entropy-based moment closures are initially attractive because of the mathematical properties they posses, most notably their robust hyperbolicity. However, for the simplified one-dimension physics considered here, it is also possible to construct many other hyperbolic closures. It was only after numerical implementation and testing of the one-dimensional maximum-entropy closure considered here that the remarkable agreement with the kinetic scheme was observed. It would be highly advantageous if other closures could provide similar accuracy without issues of realizability or the lack of an exact closed-form expression for the flux.

One set of moment equations which is hyperbolic for one-dimensional physics is the set based on Pearson-IV distribution functions recently proposed by Torrilhon [57]. For one-dimensional physics, Torrilhon proposed two hyperbolic closures. Both are 4-moment closures, and therefore, the closing relations are for $\hat{r}$, rather than $\hat{s}$. One is referred to as the "realizable" Pearson-IV closure as it possesses a realizable underlying distribution function. For this closure, the closing flux is

$$\hat{r} = 3\left(1 + \hat{q}^2 \frac{22 + \hat{q}^2}{32 - \hat{q}^2}\right). \tag{66}$$

A second variant of the Pearson-IV closure is the so-called singular closure. The underlying distribution function of this closure corresponds to a limit for the existence of the underlying Pearson-IV distribution. It leads to a closing flux of

$$\hat{r} = 3\left(1 + \frac{1}{2}\hat{q}^2\right). \tag{67}$$

Figure 14 shows the shock structure predicted by these closures for a shock wave with a Mach number of 4. It can be seen that while the agreement for the Pearson-IV-based moment closures is fairly good, it is not of the same quality as that of the maximum-entropy-based approach described earlier.

In order to reinforce the point that robust hyperbolicity is only one desirable characteristic of moment closures and that models will eventually be judged on their agreement with kinetic solutions or experiment, the poor predictive capabilities of several ad hoc globally hyperbolic closures are also now demonstrated.

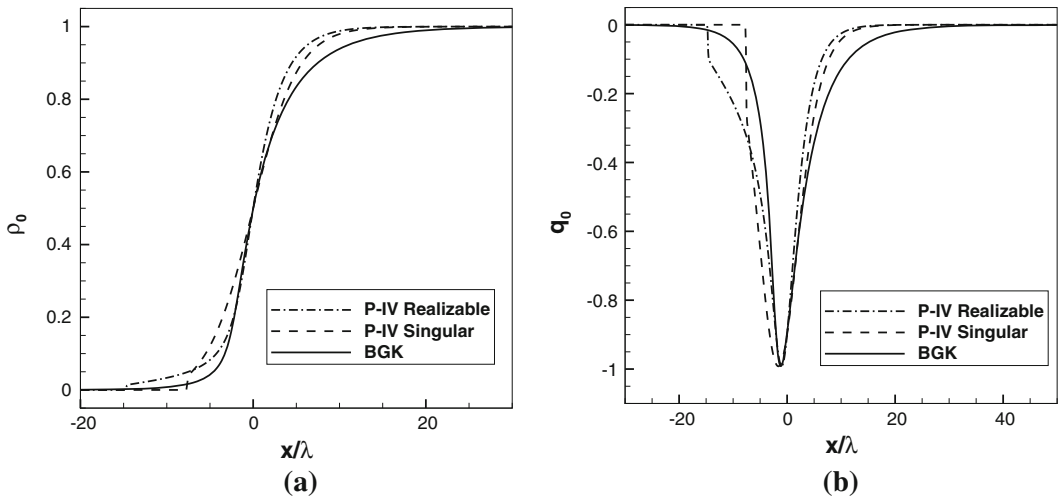

Fig. 14 Density and heat-flux profiles for a shock wave with a Mach number of 4 as predicted by the hyperbolic, one-dimensional realizable and singular Pearson-IV-based moment closures as compared to high-resolution solution of the BGK equation

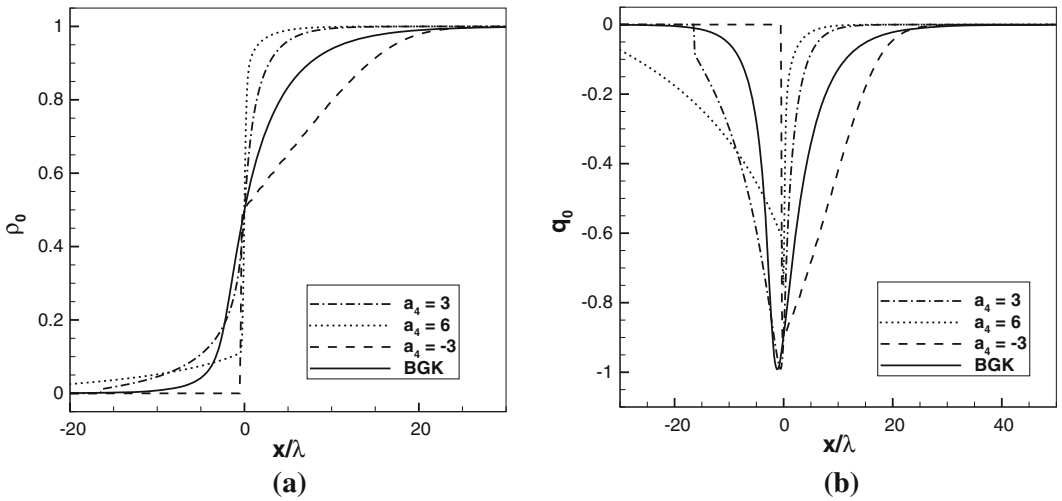

Fig. 15 Density and heat-flux profiles for a shock wave with a Mach number of 4 as predicted by several ad hoc 4-moment closures as compared to high-resolution solution of the BGK equation

These closures are constructed by assuming a polynomial form for the closing flux that possesses the correct symmetries. The flux Jacobian can then be calculated analytically and the discriminant of the characteristic equation is found. Coefficients are chosen based solely on the requirement that this discriminant be positive definite and thus the eigenvalues remain real and the closure remains globally hyperbolic. It is possible to construct 4-moment closures with a closing flux that is similar in form to the realizable Pearson-IV closure by assuming a flux of

$$\hat{r} = 3\left(1 + a_4\hat{q}^2\right). \tag{68}$$

Solutions can then be investigated for different values of a_4. Once again, a shock wave of Mach number 4 is considered in Fig. 15 for three different values of a_4 ($a_4 = 3$, $a_4 = 6$ and $a_4 = -3$). It can be seen that, as should be expected, agreement with the kinetic solution is not very good. This emphasizes the idea that strict hyperbolicity should never be the end goal in the development of moment closures. In the end, the accuracy of the model for practical non-equilibrium situations will determine its usefulness.

It is perhaps more interesting to investigate several ad hoc 5-moment closures as they have the same number of variables as the maximum-entropy closures considered herein and may provide a comparison that is more fair. The form of the closing flux considered in this work is of the form

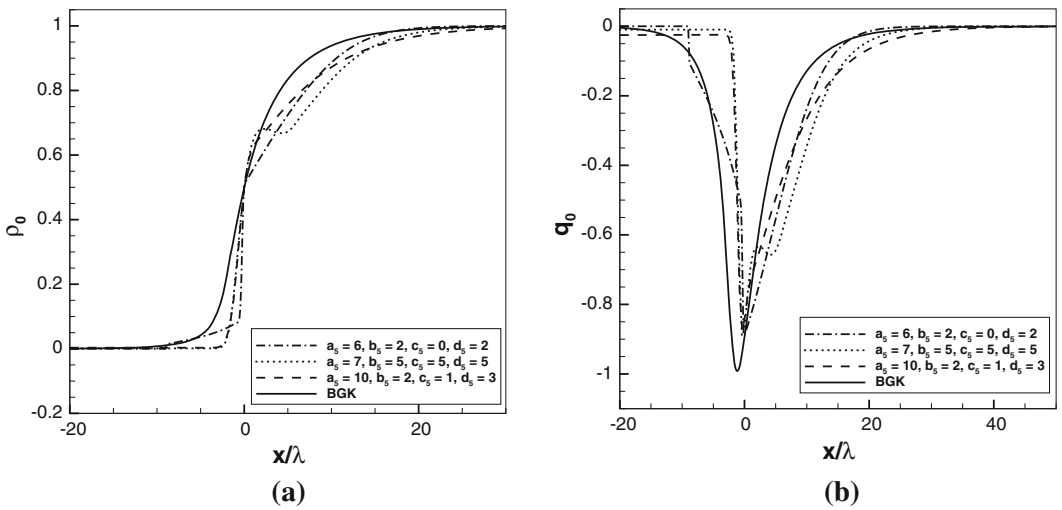

Fig. 16 Density and heat-flux profiles for a shock wave with a Mach number of 4 as predicted by several ad hoc 5-moment closures as compared to high-resolution solution of the BGK equation

$$\hat{s} = a_5\hat{q} + b_5\hat{q}(\hat{r} - 3) + c_5\hat{q}(\hat{r} - 3)^2 + d_5\hat{q}^3. \tag{69}$$

These particular terms are chosen because $\hat{s}$ must be an odd function of $\hat{q}$ for the resulting closure to have the proper symmetry. Again, three possible choices of coefficients are considered, ($a_5 = 6, b_5 = 2, c_5 = 0, d_5 = 2$), ($a_5 = 7, b_5 = 5, c_5 = 5, d_5 = 5$) and ($a_5 = 10, b_5 = 2, c_5 = 1, d_5 = 3$). In Fig. 16, the shock profiles predicted by these closures for the same shock with a Mach number of 4 are considered. Once again, it can be seen that agreement with the kinetic solution is not nearly as good as for the maximum-entropy closure, even though the number of moments is the same. Though global hyperbolicity is a desirable mathematical property for moment systems, it alone does not assure a model will be useful. The fact that maximum-entropy closures, and other closures-based thereon, are derived based on justifiable physical arguments helps to ensure that they lead to accurate predictions.

12 Conclusions

Although maximum-entropy-based moment closures are known to have several apparent disadvantages, including a lack of a closed-form expression for closing fluxes and regions of non-realizability, it has been demonstrated that these difficulties can be handled in practice, at least for some closures that contain heat transfer. Moreover, numerical predictions obtained using these closures for simple, one-dimensional situations suggest considerable promise for their use in more complex, multi-dimensional flow situations.

The preceding discussion has proposed a technique for the construction of realizable 5-moment moment closures. For this technique, the underlying distribution function is a modification of the maximum-entropy distribution function that ensures universal moment realizability for the entire range of physical validity. Global hyperbolicity has been lost; however, through careful selection of the parameter, b, moments remain numerically realizable and the closure remains hyperbolic for a very wide range non-equilibrium behaviour. The technique leads to usable moment equations; however, the cost of their numerical solution remains somewhat high. Numerical integration of distribution functions is costly, even for the one-dimensional case. For a truly three-dimensional gas, the costs associated with the resynchronization procedure would be overwhelming. However, the numerical results for the one-dimensional case shown above show the promise of hyperbolic moment closures to provide very accurate prediction of non-equilibrium flows. If such closures are going to be used as a practical tool, more computationally affordable variants are required.

It has also been shown that, for this 5-moment system, a simple surface fit can provide equally good flow predictions for the cases considered. This includes predictions for highly non-equilibrium strong shocks. Eigenvalues must still be obtained numerically; however, the cost of using the surface fit remains orders of magnitude lower than the technique of using the modified, realizable distribution function with its costly re-synchronizations.

Extension of the methods considered here to a fully three-dimensional gas is, however, not necessarily simple. It is anticipated that the modified-distribution technique of Sect. 8 will technically extend to three-dimensions. Nevertheless, the cost of the accurate numerical integration of multi-dimensional distribution functions required for the re-synchronization step is expected to be overwhelming.

If hyperbolic moment closures are to be affordable for large-scale, practical, multi-dimensional problems, closing fluxes should be expressible as a function of known moments. This was the case for the simple surface fit shown above. A three-dimensional extension of this technique would require the determination of an appropriate mapping [similar to that in Eq. (63)] after which closing fluxes can be fit easily. The challenge in this case may be that an appropriate mapping may not be obvious for multi-dimensional flows.

In summary, it seems that the issues of realizability associated with higher-order maximum-entropy moment closures for gasdynamics should be regarded as an inconvenient part of an effective model that must be addressed, rather than a problem that is chronic to a model that should be avoided.

Acknowledgments This research was supported by the Natural Sciences and Engineering Research Council of Canada. The computational resources for performing all of the calculations reported herein were provided by the SciNet High Performance Computing Consortium at the University of Toronto and Computer/Calcul Canada through funding from the Canada Foundation for Innovation (CFI) and the Province of Ontario, Canada. The first author would also like to thank the Natural Science and Engineering Research Council of Canada for their generous support through a Canadian Graduate Scholarship. The authors would like to thank the reviewers for their expert suggestions. The paper is stronger because of their efforts.

References

1. Aroian, L.A.: The fourth degree exponential distribution function. Ann. Math. Stat. **19**(4), 589–592 (1948)
2. Au, J.D.: Lösung nichtlinearer problems in der erweiterten thermodynamik. Ph.D. thesis, Technische Universität Berlin (2001)
3. Barth, T.J.: Numerical methods for gasdynamic systems on unstructured meshes. In: Kröner, M., Ohlberger, C. Rohde (eds.) An Introduction to Recent Developments in Theory and Numerics for Conservation Laws: Proceedings of the International School, vol. 5., Springer, Berlin, Freiburg (1999)
4. Barth, T.J.: On discontinuous Galerkin approximations of Boltzmann moment systems with Levermore closure. Comput. Methods Appl. Mech. Eng. **195**, 3311–3330 (2006)
5. Bhatnagar, P.L., Gross, E.P., Krook, M.: A model for collision processes in gases. I. Small amplitude processes in charged and neutral one-component systems. Phys. Rev. **94**(3), 511–525 (1954)
6. Boley, D., Luk, F., Vandevoorde, D.: Vandermonde factorization of a Hankel matrix. Paper, workshop on scientific computing 97, Hong Kong (1997)
7. Brini, F.: Hyperbolicity region in extended thermodynamics with 14 moments. Continuum Mech. Thermodyn. **13**, 1–8 (2001)
8. Brown, S.L.: Approximate Riemann solvers for moment models of dilute gases. Ph.D. thesis, University of Michigan (1996)
9. Brown, S.L., Roe, P.L., Groth, C.P.T.: Numerical solution of a 10-moment model for nonequilibrium gasdynamics. Paper 95-1677, AIAA (1995)
10. Burgers, J.M.: Flow Equations for Composite Gases. Academic Press, New York, NY (1969)
11. Chapman, S., Cowling, T.G.: The Mathematical Theory of Non-uniform Gases. Cambridge University Press, Cambridge (1960)
12. Dreyer, W.: Maximization of the entropy in non-equilibrium. J. Phys. A: Math. Gen. **20**, 6505–6517 (1987)
13. Feldmann, S., Heinig, G.: Vandermonde factorization and canonical representations of block Hankel matrices. In: Proceedings of the Fourth Conference of the International Linear Algebra Society. Linear Algebra Appl. **241–243**, 247–278 (1996). doi:10.1016/0024-3795(95)00501-3
14. Friedrichs, K.O., Lax, P.D.: Systems of conservation laws with a convex extension. ProcNAS **68**, 1686–1688 (1971)
15. Godunov, S.K.: Finite-difference method for numerical computations of discontinuous solutions of the equations of fluid dynamics. Mat. Sb. **47**, 271–306 (1959)
16. Godunov, S.K.: An interesting class of quasilinear systems. Sov. Math. Dokl. **2**, 947–949 (1961)
17. Gombosi, T.I.: Gaskinetic Theory. Cambridge University Press, Cambridge (1994)
18. Grad, H.: On the kinetic theory of rarefied gases. Commun. Pure Appl. Math. **2**, 331–407 (1949)
19. Groth, C.P.T., McDonald, J.G.: Towards physically-realizable and hyperbolic moment closures for kinetic theory. Continuum Mech. Thermodyn. **21**, 467–493 (2009)
20. Hamburger, H.L.: Hermitian transformations of deficiency-index (1, 1), Jacobian matrices, and undetermined moment problems. Am. J. Math. **66**, 489–552 (1944)
21. Harten, A., Lax, P.D., van Leer, B.: On upstream differencing and Godunov-type schemes for hyperbolic conservation laws. SIAM Rev. **25**(1), 35–61 (1983)
22. Hauck, C.D., Levermore, C.D., Tits, A.L.: Convex duality and entropy-based moment closures: Characterizing degenerate densities. SIAM J. Control Opt. **47**(4), 1977–2015 (2008)
23. Hertweck, F.: Allgemeine 13-momenten-näherung zur Fokker–Planck–Gleichung eines plasmas. Zeitschrift für Naturforschung **20a**, 1243–1255 (1965)
24. Holway, L.H.: Approximation procedures for kinetic theory. Ph.D. thesis, Harvard University (1963)
25. Holway, L.H.: Kinetic theory of shock structure using an ellipsoidal distribution function. In: de Leeuw, J.H. (ed.) Rarefied Gas Dynamics, vol. I., pp. 193–215. Academic Press, New York, NY (1966)
26. Holway, L.H.: New statistical models for kinetic theory: methods of construction. Phys. Fluids **9**(9), 1658–1673 (1966)
27. Holway, L.H.: The effect of collisional models upon shock wave structure. In: Brundin, C.L. (ed.) Rarefied Gas Dynamics, vol. I., pp. 759–784. Academic Press, New York, NY (1967)
28. Junk, M.: Minimum relative entropy systems of the Boltzmann equation. Unpublished work
29. Junk, M.: Domain of definition of Levermore's five-moment system. J. Stat. Phys. **93**(5/6), 1143–1167 (1998)
30. Junk, M.: Maximum entropy moment systems and Galilean invariance. Continuum Mech. Thermodyn. **14**, 563–576 (2002)
31. Junk, M.: Maximum entropy moment problems and extended Euler equations. In: proceedings of IMA Workshop "Simulation of Transport in Transition Regimes", IMA Volume in Mathematics and Its Applications, vol. 135, pp. 189–198. Springer (2004)
32. Levermore, C.D.: Moment closure hierarchies for kinetic theories. J. Stat. Phys. **83**, 1021–1065 (1996)
33. Matz, A.W.: Maximum likelihood parameter estimation for the quartic exponential distribution. Technometrics **20**(4), 475–484 (1978)
34. Maxwell, J.C.: On the dynamical theory of gases. Philos. Trans. R. Soc. Lond. **157**, 49–88 (1867)
35. McDonald, J.G.: Extended fluid-dynamic modelling for numerical solution of micro-scale flows. Ph.D. thesis, University of Toronto (2011)
36. McDonald, J.G., Groth, C.P.T.: Numerical modeling of micron-scale flows using the Gaussian moment closure. Paper 2005-5035, AIAA (2005)
37. McDonald, J.G., Groth, C.P.T.: Extended fluid-dynamic model for micron-scale flows based on Gaussian moment closure. Paper 2008-0691, AIAA (2008)
38. McDonald, J.G., Sachdev, J.S., Groth, C.P.T.: Gaussian moment closure for the modelling of continuum and micron-scale flows with moving boundaries. In: Deconinck, H., Dick, E. (eds.) Proceedings of the Fourth International Conference on Computational Fluid Dynamics, ICCFD4, Ghent, Belgium, 10–14 July 2006, pp. 783–788. Springer, Heidelberg (2009)
39. Mieussens, L.: Discrete velocity model and implicit scheme for the BGK equation of rarefied gas dynamics. Math. Models Methods Appl. Sci. **10**(8), 1121–1149 (2000)
40. Müller, I., Reitebuch, D., Weiss, W.: Extended thermodynamics—consistent in order of magnitude. Continuum Mech. Thermodyn. **15**, 113–146 (2003)

41. Müller, I., Ruggeri, T.: Rational Extended Thermodynamics. Springer, New York, NY (1998)
42. Oraevskii, V., Chodura, R., Feneberg, W.: Hydrodynamic equations for plasmas in strong magnetic fields—i collisionless approximation. Plasma Phys. **10**, 819–828 (1968)
43. O'Toole, A.L.: A method of determining the constants in the bimodal fourth degree exponential function. Ann. Math. Stat. **4**(2), 79–93 (1933)
44. O'Toole, A.L.: On the system of curves for which the method of moments is the best method of fitting. Ann. Math. Stat. **4**(1), 1–29 (1933)
45. Reed, M., Simon, B.: Methods of Modern Mathematical Physics, II: Fourier Analysis, Self-adjointness. Academic Press, New York, NY (1975)
46. Sachdev, J.S.: Parallel solution-adaptive method for predicting solid propellant rocket motor core flows. Ph.D. thesis, University of Toronto (2007)
47. Sachdev, J.S., Groth, C.P.T.: A mesh adjustment scheme for embedded boundaries. Commun. Comput. Phys. **2**(6), 1095–1124 (2007)
48. Sachdev, J.S., Groth, C.P.T., Gottlieb, J.J.: Parallel AMR scheme for turbulent multi-phase rocket motor core flows. Paper 2005-5334, AIAA (2005)
49. Schneider, J.: Entropic approximation in kinetic theory. Math. Model. Numer. Anal. **38**(3), 541–561 (2004)
50. Struchtrup, H.: Stable transport equations for rarefied gases at high orders in the Knudsen number. Phys. Fluids **16**(11), 3921–3934 (2004)
51. Struchtrup, H.: Macroscopic Transport Equations for Rarefied Gas Flows. Springer, Berlin (2005)
52. Struchtrup, H., Torrilhon, M.: Regularization of Grad's 13 moment equations: derivation and linear analysis. Phys. Fluids **15**, 2668–2680 (2003)
53. Struchtrup, H., Torrilhon, M.: H theorem, regularization, and boundary conditions for the linearized 13 moment equations. Phys. Rev. Lett. **99**, 014502 (2007)
54. Suzuki, Y., van Leer, B.: Application of the 10-moment model to MEMS flows. Paper 2005-1398, AIAA (2005)
55. Tallec, P.L., Perlat, J.P.: Numerical analysis of Levermore's moment system. Technical report 3124, INRIA Rocquencourt (1997)
56. Torrilhon, M.: Characteristic waves and dissipation in the 13-moment-case. Continuum Mech. Thermodyn. **12**, 289–301 (2000)
57. Torrilhon, M.: Hyperbolic moment equations in kinetic gas theory based on multi-variate Pearson-IV-distributions. Commun. Comput. Phys. **7**(4), 639–673 (2010)
58. Torrilhon, M., Struchtrup, H.: Boundary conditions for regularized 13 moment equations for micro-channel-flows. J. Comput. Phys. **227**, 1982–2011 (2008)